Bias-dependent model of the electrical impedance of ionic polymer-metal composites

Youngsu Cha and Maurizio Porfiri

Phys. Rev. E **87**, 022403 — Published 6 February 2013

DOI: 10.1103/PhysRevE.87.022403

A bias-dependent model of the electrical impedance of ionic polymer metal composites

Youngsu Cha[1] and Maurizio Porfiri[1,*]

[1] *Department of Mechanical and Aerospace Engineering, Polytechnic Institute of New York University Brooklyn, NY, 11201 USA*

In this paper, we analyze the charge dynamics of ionic polymer metal composites (IPMCs) in response to voltage inputs composed of a large DC bias and a small superimposed time-varying voltage. The IPMC chemoelectrical behavior is described through the modified Poisson-Nernst-Planck framework, in which steric effects are taken into consideration. The physics of charge build up and mass transfer in the proximity of the high surface electrodes is modeled by schematizing the IPMC as the stacked sequence of five layers, in which the ionomeric membrane is separated from the metal electrodes by two composite layers. The method of matched asymptotic expansions is used to derive a semianalytical solution for the concentration of mobile counterions and the electric potential in the IPMC, which is, in turn, used to establish an equivalent circuit model for the IPMC electrical response. The circuit model consists of the series connection of a resistor and two complex elements, each constituted by the parallel connection of a capacitor and a Warburg impedance. The resistor is associated with ion transport in the ionomeric membrane and is independent of the DC bias. The capacitors and the Warburg impedance idealize charge build up and mass transfer in the vicinity of the electrodes and their value is controlled by the DC bias. The proposed approach is validated against experimental results on in-house fabricated IPMCs and the accuracy of the equivalent circuit is assessed through comparison with finite element results.

PACS numbers: 46.15.Ff, 68.35.Fx 82.45.Wx, 82.47.Gh,

I. INTRODUCTION

Ionic polymer metal composites (IPMCs) are a novel class of electroactive materials which find application as sensors [1–5], actuators [6–11], and energy harvesters [12–18]. In their fundamental incarnation, IPMCs consist of an electrically charged polymer (ionomeric) membrane that is infused with a solvent, neutralized by mobile counterions, and plated by noble metal electrodes [19].

IPMC fabrication is generally based on an electroless chemical reduction process [20, 21] consisting of the diffusion and adsorption of a metal salt in the ionomer and its consecutive deposition at the ionomer surface through a reducing agent. Electrode deposition seldom results in the formation of a highly heterogeneous layer, whose conductive and dielectric properties differ from both the polymer and the metal salt [22–26]. Charge redistribution in the vicinity of such regions is considered to be a primary factor in both IPMC actuation [27–30] and sensing [31–34]. In [24], we have presented the notion of "composite layer" to describe IPMC charge transport at the ionomer-electrode interface, building on physical insight offered by the concepts of inner electrode [25], intermediate layer [26], and active area model [22, 23].

Specifically, we have proposed a new physics-based model for IPMC chemoelectrical behavior based on the integration of the composite layer concept within the Poisson-Nernst-Planck (PNP) framework [28, 35–43]. In this model, the IPMC is described as a stacked sequence of five homogeneous layers, wherein the ionomeric membrane is separated from the metal electrodes by two composite layers. From the analysis of the linearized PNP system, we have demonstrated that IPMC response can be described through a classical Randles circuit model, see for example [44], consisting of a resistor, a capacitor, and a Warburg impedance as suggested in [19, 45]. The capacitor idealizes the phenomena of charge build up in the double layer region, the Warburg impedance is related to mass transfer at the interfaces, and the resistor is associated with ion transport in the ionomer bulk. In agreement with the majority of experimental observations in the literature, see for example [42, 46–48], the model predicts that the impedance magnitude decreases with a slope of approximately $-10\,\mathrm{dB/decade}$ at low frequency and reaches an almost constant value for high frequency. The accuracy of the model has been validated through experimental results on Nafion-based IPMCs and comparison with alternative models for IPMC impedance [49–51].

In this paper, we extend this framework to study IPMC impedance in response to an applied DC voltage bias. We use a modified PNP formulation to account for the presence of steric effects [52–54], which are shown to play a prominent role in shaping the charge distribution in the composite layers at moderately large voltages, see also the comprehensive review in [55]. Following [37, 40, 52–54, 56–60], we use the method of matched asymptotic expansions, see for example [61], to derive a semi-analytical solution for the electric potential and the charge concentration in the IPMC along with a new circuit model for IPMCs in presence of a DC voltage bias. The equivalent circuit model consists of the series connection of two impedances of the form presented in [24] to account for differences in charge build up at the anode and cathode regions for large voltages. We demonstrate that the

* mporfiri@poly.edu; http://faculty.poly.edu/ mporfiri/index.htm

relative thickness of the composite layer with respect to the ionomer thickness has a major influence on IPMC impedance. Specifically, we find that increasing the DC bias dramatically reduces double-layer phenomena and mass transport for thin composite layers, whereas, the DC bias has a secondary effect on IPMC chemoelectrical behavior for thick composite layers. The asymptotic solution is verified through comparison with finite element results and the overall modeling approach is validated against experimental results on Nafion-based IPMC samples for DC voltages in the range $0 - 0.5\,\mathrm{V}$. Notably, the effect of DC bias on IPMC impedance has been recently investigated in [42] by using an approximate solution of the classical PNP system in absence of steric effects and mass transfer at the ionomer-electrode interface. A power series expansion is therein used to describe experimental results for DC bias in the range $0 - 1.5\,\mathrm{V}$.

We organize the paper as follows. In Section II, we present the governing equations for the chemoelectrical response of the IPMC. In Section III, we study IPMC response to a small voltage applied across the electrodes. In Section IV, we analyze IPMC response to a DC bias and a superimposed small AC voltage. In Section V, we verify the semianalytical solution through finite element results and offer some validation of the model through comparison with experimental result. Conclusions are reported in Section VI.

II. GOVERNING EQUATIONS

We model the IPMC as a stacked sequence of five layers, comprising an ionomer core, two metal electrodes, and two composite layers, see Figure 1. We assume that the metal electrodes are perfect conductor. The composite layers are treated as identical ionomers of length d with highly dissimilar electrical properties than the ionomer core, due to the presence of scattered metal particles. To account for the high surface of the electrodes, we assume that the permittivity of the ionomer core varies along its thickness $2h$. Specifically, we hypothesize that the permittivity attains larger values in the vicinity of the composite layers.

In this framework, IPMC chemoelectrical behavior can be modeled by focusing on the time evolution of the counterion concentration and the electrical potential along the x direction, see for example [36, 37, 40]. The center of the ionomer is set as the origin of the abscissa x so that $-h \leq x \leq h$ identifies the polymer region and $h < x \leq h + d$ and $-(h + d) \leq x < -h$ refer to the right and left composite layers, respectively.

A. Ionomeric membrane

We use the modified PNP formulation to describe the evolution of the counterion concentration per unit hydrated polymer $c(x,t)$ and the electrical potential $\psi(x,t)$

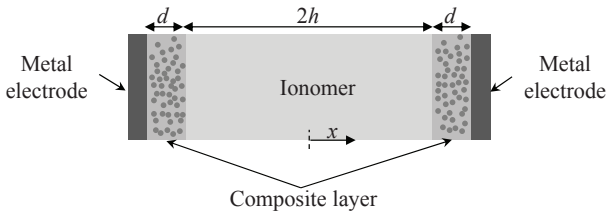

FIG. 1. Schematics of the IPMC.

in the ionomer core, see for example [52–54]. The mobile counterion has positive charge and unitary valency and anions with same valency are fixed to the backbone polymer.

In this framework, the distribution of $\psi(x,t)$ is described by the Gauss law

$$\frac{\partial \mathcal{D}(x,t)}{\partial x} = F[c(x,t) - c_0] \tag{1}$$

where $\mathcal{D}(x,t)$ is the component of the electric displacement along the x direction, c_0 is the concentration of fixed anion per unit IPMC volume (assumed to be constant), and F is the Faraday constant. The electric displacement is related to the electric potential through its constitutive behavior, that is,

$$\mathcal{D}(x,t) = -\epsilon(x)\frac{\partial \psi(x,t)}{\partial x} \tag{2}$$

where $\epsilon(x)$ is the permittivity of the polymer. In this study, we assume the following dependence for $\epsilon(x)$

$$\epsilon(x) = (\epsilon_\mathrm{i} - \epsilon_\mathrm{b})e^{-\mu\frac{h+x}{h}} + (\epsilon_\mathrm{i} - \epsilon_\mathrm{b})e^{-\mu\frac{h-x}{h}} + \epsilon_\mathrm{b} \tag{3}$$

where ϵ_i and ϵ_b quantify the permittivity of the ionomer at the interface with the composite layer and in the bulk, respectively, and μ measures the rate of decay of the permittivity, see for example Figure 2. By combining (1) and (2), we obtain the Poisson equation connecting the electric potential with the counterion concentration in the ionomer

$$-\frac{\partial}{\partial x}\left(\epsilon(x)\frac{\partial \psi(x,t)}{\partial x}\right) = F[c(x,t) - c_0] \tag{4}$$

The mass balance for the mobile counterions is

$$\frac{\partial c(x,t)}{\partial t} = -\frac{\partial J(x,t)}{\partial x} \tag{5}$$

where $J(x,t)$ is the counterion flux. Such flux is affected by the counterion diffusion and electromigration according to the modified Nernst-Planck constitutive equation that accounts for steric effects [52–54], namely,

$$J(x,t) = -D\left[\frac{c_0}{c_0 - \nu c(x,t)}\frac{\partial c(x,t)}{\partial x} + \frac{Fc(x,t)}{\mathcal{R}T}\frac{\partial \psi(x,t)}{\partial x}\right] \tag{6}$$

where D is the diffusivity of the mobile counterions in the polymer (assumed to be constant), $\mathcal{R}$ is the universal

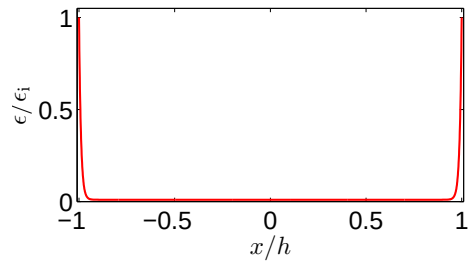

FIG. 2. (Color online) Permittivity on the ionomer core scaled by the permittivity at the interface $x = \pm h$ for the representative parameters $\epsilon_i/\epsilon_b = 100$ and $\mu = 100$.

gas constant, and T is the absolute IPMC temperature. Here, $\nu = c_0 a^3 N$ is a dimensionless positive parameter measuring the concentration packing limit and varying between 0 and 1 [52–54], with N being the Avogadro's number ($6.0221 \times 10^{23}\,\mathrm{mol}^{-1}$) and a the spacing between the ions. The steric effect imposes that the concentration of mobile counterions in the polymer cannot exceed c_0/ν [52–54]. By substituting (6) into (5), we obtain the modified Nernst-Planck equation, that is,

$$\frac{\partial c(x,t)}{\partial t} = D\frac{\partial}{\partial x}\left[\frac{c_0}{c_0 - \nu c(x,t)}\frac{\partial c(x,t)}{\partial x} + \frac{F c(x,t)}{\mathcal{R}T}\frac{\partial \psi(x,t)}{\partial x}\right] \tag{7}$$

Equations (4) and (7) are referred to as the modified PNP system for the ionomer core. Further insight on the modified PNP framework can be found in [62] including the influence of steric phenomena on the ion diffusivity, that is not accounted for in our analysis.

B. Composite layers

The modified PNP system for the composite layers is derived following an analogous procedure. For convenience, we refer to all the pertinent variables therein using the subscript "cl". Specifically, we use ϵ_{cl} and D_{cl} to identify the dielectric constant and the diffusivity, which are both assumed to be constant and different than the ionomer properties. Moreover, we use a subscript $\pm$ to identify the field variables in the two composite layers.

In the composite layers, the Poisson equation reads

$$-\epsilon_{\mathrm{cl}}\frac{\partial^2 \psi_{\mathrm{cl}\pm}(x,t)}{\partial x^2} = F[c_{\mathrm{cl}\pm}(x,t) - c_0\phi] \tag{8}$$

where ϕ is the volume fraction of the ionomer material in the composite layer [24] and $\mathcal{D}_{\mathrm{cl}\pm}(x,t)$ equals $-\epsilon_{\mathrm{cl}}\partial\psi_{\mathrm{cl}\pm}(x,t)/\partial x$. The modified Nernst-Planck equation in the composite layer is

$$\frac{\partial c_{\mathrm{cl}\pm}(x,t)}{\partial t} = D_{\mathrm{cl}}\frac{\partial}{\partial x}\left[\frac{c_0\phi}{c_0\phi - \nu c_{\mathrm{cl}\pm}(x,t)}\frac{\partial c_{\mathrm{cl}\pm}(x,t)}{\partial x} + \frac{F c_{\mathrm{cl}\pm}(x,t)}{\mathcal{R}T}\frac{\partial \psi_{\mathrm{cl}\pm}(x,t)}{\partial x}\right] \tag{9}$$

We comment that the steric effect is not varied with respect to the ionomer core, since it is related to the counterion size. Moreover, we note that the electron flux in the composite layers is neglected based on the experimental results reported in [24], which show that electron transport is a secondary phenomenon in the charge dynamics in the composite layers.

C. Boundary, interface, and initial conditions

At the interface between the ionomer core and the composite layers, $x = \pm h$, we enforce the continuity of counterion concentration, electric potential, counterion flux, and electric displacement, that is, we set

$$c(\pm h,t) = c_{\mathrm{cl}\pm}(\pm h,t)/\phi \tag{10a}$$
$$\psi(\pm h,t) = \psi_{\mathrm{cl}\pm}(\pm h,t) \tag{10b}$$
$$J(\pm h,t) = J_{\mathrm{cl}\pm}(\pm h,t) \tag{10c}$$
$$\mathcal{D}(\pm h,t) = \mathcal{D}_{\mathrm{cl}\pm}(\pm h,t) \tag{10d}$$

In this study, we focus on the chemoelectrical response of IPMCs under a voltage difference applied across the electrodes, which are assumed to be ion-blocking, see for example [37]. Therefore, we impose the following boundary conditions at $x = \pm(h+d)$

$$\psi_{\mathrm{cl}\pm}(\pm(h+d),t) = \pm\frac{V(t)}{2} \tag{11a}$$
$$J_{\mathrm{cl}\pm}(\pm(h+d),t) = 0 \tag{11b}$$

We further assume that the whole IPMC is initially electroneutral, that is,

$$c(x,0) = c_0 \tag{12a}$$
$$c_{\mathrm{cl}\pm}(x,0)/\phi = c_0 \tag{12b}$$

We note that ion-blocking conditions impose that the total net charge in the IPMC is always zero and that

$$\mathcal{D}_{\mathrm{cl}+}(h+d,t) = \mathcal{D}_{\mathrm{cl}-}(-h-d,t) \tag{13}$$

Further important properties of the PNP system can be found in [63].

D. Current

As the voltage $V(t)$ is applied across the IPMC electrodes, a current is generated through the IPMC. Such

current is composed of a displacement current and a conduction current due to counterion flux [64] and its value is independent of x. By denoting this current as $I(t)$, we have

$$I(t) = -\left[\frac{\partial \mathcal{D}(x,t)}{\partial t} + FJ(x,t)\right] \tag{14a}$$

$$I(t) = -\left[\frac{\partial \mathcal{D}_{\mathrm{cl}\pm}(x,t)}{\partial t} + FJ_{\mathrm{cl}\pm}(x,t)\right] \tag{14b}$$

in the ionomer and the composite layers, respectively. Note that if x is taken to be at the electrode-composite layer interface, the jump in the electric displacement should be considered in place of the first summand in (14) and the second summand is zero due to the ion-blocking electrodes.

E. Nondimensional equations

We nondimensionalize the governing equations in the ionomer core by scaling $\psi(x,t)$ and $c(x,t)$ with respect to the thermal voltage $\mathcal{R}T/F$ and the fixed anion concentration with respect to c_0, respectively. Furthermore, the spatial abscissa and the time variable are nondimensionlized using the ionomer semithickness h and the time constant

$$\tau = \frac{h}{FD}\sqrt{\frac{\epsilon_{\mathrm{i}}\mathcal{R}T}{c_0}} \tag{15}$$

The dimensionless form of the modified PNP system in (4) and (7) is

$$-\delta^2 \frac{\partial}{\partial \tilde{x}}\left(\frac{\epsilon(\tilde{x})}{\epsilon_{\mathrm{i}}}\frac{\partial \tilde{\psi}(\tilde{x},\tilde{t})}{\partial \tilde{x}}\right) = \tilde{c}(\tilde{x},\tilde{t}) - 1 \tag{16a}$$

$$\frac{\partial \tilde{c}(\tilde{x},\tilde{t})}{\partial \tilde{t}} = \delta \frac{\partial}{\partial \tilde{x}}\left[\frac{1}{1-\nu\tilde{c}(\tilde{x},\tilde{t})}\frac{\partial \tilde{c}(\tilde{x},\tilde{t})}{\partial \tilde{x}} + \tilde{c}(\tilde{x},\tilde{t})\frac{\partial \tilde{\psi}(\tilde{x},\tilde{t})}{\partial \tilde{x}}\right] \tag{16b}$$

where nondimensional variables are indicated with superimposed tilde and

$$\delta = \frac{1}{Fh}\sqrt{\frac{\epsilon_{\mathrm{i}}\mathcal{R}T}{c_0}} \tag{17}$$

The parameter δ measures the ratio between the so-called Debye screening length $\lambda = \sqrt{(\epsilon_{\mathrm{i}}\mathcal{R}T)/(F^2c_0)}$, that quantifies the thickness of the diffuse charge layers at the ionomer-electrode interface, and the ionomer core semithickness, see also [37]. Such parameter is much smaller than one for typical IPMCs, see for example [36, 37, 40].

In the composite layer, we use a similar nondimensionalization. Specifically, we scale again the electric potential by the thermal voltage and the counterion concentration by $c_0\phi$. Moreover, the spatial domain is nondimensionalized using $r_\pm = (h + d \mp x)/(h\sqrt{\delta})$ to magnify the composite layer thickness, where we assume that d^2 is on the order of λh. This implies that the composite layer is simultaneously wider than the Debye screening length and narrower than the ionomer core, so that the chemolectrical behavior is therein affected by both faradaic and mass transport effects. The dimensionless forms of the PNP system in (8) and (9) are

$$-\epsilon^* \frac{\partial^2 \tilde{\psi}_{\mathrm{cl}\pm}(r_\pm,\tilde{t})}{\partial (r_\pm)^2} = \tilde{c}_{\mathrm{cl}\pm}(r_\pm,\tilde{t}) - 1 \tag{18a}$$

$$\frac{\partial \tilde{c}_{\mathrm{cl}\pm}(r_\pm,\tilde{t})}{\partial \tilde{t}} = D^*\delta \frac{\partial}{\partial r_\pm}\left[\frac{1}{1-\nu\tilde{c}_{\mathrm{cl}\pm}(r_\pm,\tilde{t})}\frac{\partial \tilde{c}_{\mathrm{cl}\pm}(r_\pm,\tilde{t})}{\partial r_\pm} + \tilde{c}_{\mathrm{cl}\pm}(r_\pm,\tilde{t})\frac{\partial \tilde{\psi}_{\mathrm{cl}\pm}(r_\pm,\tilde{t})}{\partial r_\pm}\right] \tag{18b}$$

where $\epsilon^* = \epsilon_{\mathrm{cl}}\delta/(\epsilon_{\mathrm{i}}\phi)$ and $D^* = D_{\mathrm{cl}}/(D\delta)$. We assume that ϵ^* and D^* are on the order of the unity based on the assumptions of higher permittivity and lower diffusivity in the composite layer than the ionomer core [24]. Moreover, we hypothesize that $\mu \ll 1/\delta$, so that the charge boundary layer is considerably thinner than the decay length of the permittivity of the ionomer core.

Additionally, the nondimensional boundary and initial conditions are

$$\tilde{c}(\pm 1,\tilde{t}) = \tilde{c}_{\mathrm{cl}\pm}(d^*,\tilde{t}) \tag{19a}$$

$$\tilde{\psi}(\pm 1,\tilde{t}) = \tilde{\psi}_{\mathrm{cl}\pm}(d^*,\tilde{t}) \tag{19b}$$

$$\tilde{J}(\pm 1,\tilde{t}) = \tilde{J}_{\mathrm{cl}\pm}(d^*,\tilde{t}) \tag{19c}$$

$$\tilde{\mathcal{D}}(\pm 1,\tilde{t}) = \tilde{\mathcal{D}}_{\mathrm{cl}\pm}(d^*,\tilde{t}) \tag{19d}$$

$$\tilde{\psi}_{\mathrm{cl}\pm}(0,\tilde{t}) = \pm\alpha(\tilde{t})/2 \tag{19e}$$

$$\tilde{J}_{\mathrm{cl}\pm}(0,\tilde{t}) = 0 \tag{19f}$$

$$\tilde{c}(\tilde{x},0) = 1 \tag{19g}$$

$$\tilde{c}_{\mathrm{cl}\pm}(r_\pm,0) = 1 \tag{19h}$$

where the thickness of the composite layer d and the applied voltage $V(t)$ across the electrodes are nondimensionlized as $d^* = d/(h\sqrt{\delta})$ and $\alpha(\tilde{t}) = FV(t)/(\mathcal{R}T)$, respectively.

When comparing the modified PNP systems for the ionomer core and for the composite layers in (16) and (18), we note that both systems are singularly perturbed. Specifically, both the Poisson and the modified Nernst-Planck equations are singularly perturbed in the polymer core and only the modified Nernst-Planck equation is singularly perturbed in the composite layers. The power of δ differs in the two modified PNP sets, with a power 2 for the ionomer core and a power 1 for the composite layers.

III. ANALYSIS FOR SMALL VOLTAGE INPUTS

A. Linearized equations

We consider the IPMC response to an applied voltage that is considerably smaller than the thermal volt-

age, so that, $\alpha(\tilde{t}) \ll 1$. In this case, the nondimensional modified Nernst-Planck equation in (16b) and (18b) can be linearized following [24]. Specifically, we linearize in the neighborhood of the equilibrium configuration defined by $\tilde{\psi}(\tilde{x},\tilde{t}) = 0$, $\tilde{\psi}_{\mathrm{cl}\pm}(r_\pm,\tilde{t}) = 0$, $\tilde{c}(\tilde{x},\tilde{t}) = 1$, and $\tilde{c}_{\mathrm{cl}\pm}(r_\pm,\tilde{t}) = 1$, so that (16b) and (18b) become

$$\frac{\partial \tilde{c}(\tilde{x},\tilde{t})}{\partial \tilde{t}} = \delta\left[\frac{1}{1-\nu}\frac{\partial^2 \tilde{c}(\tilde{x},\tilde{t})}{\partial \tilde{x}^2} + \frac{\partial^2 \tilde{\psi}(\tilde{x},\tilde{t})}{\partial \tilde{x}^2}\right] \tag{20a}$$

$$\frac{\partial \tilde{c}_{\mathrm{cl}\pm}(r_\pm,\tilde{t})}{\partial \tilde{t}} = D^*\delta\left[\frac{1}{1-\nu}\frac{\partial^2 \tilde{c}_{\mathrm{cl}\pm}(r_\pm,\tilde{t})}{\partial (r_\pm)^2} + \frac{\partial^2 \tilde{\psi}_{\mathrm{cl}\pm}(r_\pm,\tilde{t})}{\partial (r_\pm)^2}\right] \tag{20b}$$

B. Outer expansion in the ionomer

In the ionomer core, we seek regular asymptotic expansions for both the concentration and the electric potential, that is,

$$\tilde{c}^{\circ}(\tilde{x},\tilde{t}) = \tilde{c}_0^{\circ}(\tilde{x},\tilde{t}) + \delta\tilde{c}_1^{\circ}(\tilde{x},\tilde{t}) + \dots \tag{21a}$$

$$\tilde{\psi}^{\circ}(\tilde{x},\tilde{t}) = \tilde{\psi}_0^{\circ}(\tilde{x},\tilde{t}) + \delta\tilde{\psi}_1^{\circ}(\tilde{x},\tilde{t}) + \dots \tag{21b}$$

where superscript $\circ$ refers to the outer solution.

By substituting (21) into the nondimensional modified PNP system in (16a) and (20a), adapting the initial condition (19g), and equating summands with the same power of δ, we obtain a hierarchy of partial differential equations. At the leading order, we find the following general solution

$$\tilde{c}_0^{\circ}(\tilde{x},\tilde{t}) = 1 \tag{22a}$$

$$\tilde{\psi}_0^{\circ}(\tilde{x},\tilde{t}) = A_1(\tilde{t})\tilde{x} + A_2(\tilde{t}) \tag{22b}$$

where $A_1(\tilde{t})$ and $A_2(\tilde{t})$ are unknown functions of time. Due to the linearity of the problem, the concentration and electric potential profiles are odd functions of x, see also [24], thus, we let $A_2(\tilde{t}) = 0$.

C. Inner expansion in the ionomer

The outer expansion is close to the exact solution everywhere in the ionomer core except of the ionomer-composite layer interfaces, where boundary layers are expected to develop, see for example [28, 36, 37]. In these regions, we perform the following change of variable

$$\xi^{\pm} = \frac{1 \mp \tilde{x}}{\delta} \tag{23}$$

where superscripts $+$ and $-$ identify interfaces proximal to $\tilde{x} = +1$ and $\tilde{x} = -1$, respectively. By substituting the local variable $\xi^{\pm}$ into the modified PNP system in (16a) and (20a) and taking the limit of $\epsilon(\tilde{x})$ for small δ, we find

$$-\delta\mu\frac{\epsilon_{\mathrm{i}} - \epsilon_{\mathrm{b}}}{\epsilon_{\mathrm{i}}}\frac{\partial \tilde{\psi}^{\pm}(\xi^{\pm},\tilde{t})}{\partial(\xi^{\pm})} - \frac{\partial^2 \tilde{\psi}^{\pm}(\xi^{\pm},\tilde{t})}{\partial(\xi^{\pm})^2} = \tilde{c}^{\pm}(\xi^{\pm},\tilde{t}) - 1 \tag{24a}$$

$$\delta\frac{\partial \tilde{c}^{\pm}(\xi^{\pm},\tilde{t})}{\partial \tilde{t}} = \frac{1}{1-\nu}\frac{\partial^2 \tilde{c}^{\pm}(\xi^{\pm},\tilde{t})}{\partial(\xi^{\pm})^2} + \frac{\partial^2 \tilde{\psi}^{\pm}(\xi^{\pm},\tilde{t})}{\partial(\xi^{\pm})^2} \tag{24b}$$

We note that varying the profile of the permittivity does not influence the governing equations, provided that the Debye screening length is sufficiently smaller than the scale of variation of the dielectric permittivity.

In the inner regions, we seek regular asymptotic expansions of the form

$$\tilde{c}^{\pm}(\xi^{\pm},\tilde{t}) = \tilde{c}_0^{\pm}(\xi^{\pm},\tilde{t}) + \delta\tilde{c}_1^{\pm}(\xi^{\pm},\tilde{t}) + \dots \tag{25a}$$

$$\tilde{\psi}^{\pm}(\xi^{\pm},\tilde{t}) = \tilde{\psi}_0^{\pm}(\xi^{\pm},\tilde{t}) + \delta\tilde{\psi}_1^{\pm}(\xi^{\pm},\tilde{t}) + \dots \tag{25b}$$

By substituting the expansion in (25) in the PNP system (24), we obtain the following leading order equations

$$-\frac{\partial^2 \tilde{\psi}_0^{\pm}(\xi^{\pm},\tilde{t})}{\partial(\xi^{\pm})^2} = \tilde{c}_0^{\pm}(\xi^{\pm},\tilde{t}) - 1 \tag{26a}$$

$$\frac{1}{1-\nu}\frac{\partial^2 \tilde{c}_0^{\pm}(\xi^{\pm},\tilde{t})}{\partial(\xi^{\pm})^2} + \frac{\partial^2 \tilde{\psi}_0^{\pm}(\xi^{\pm},\tilde{t})}{\partial(\xi^{\pm})^2} = 0 \tag{26b}$$

The general solution of such system is

$$\tilde{c}_0^{\pm}(\xi^{\pm},\tilde{t}) = 1 \mp A_3(\tilde{t})e^{-\xi^{\pm}\sqrt{1-\nu}} \mp A_4(\tilde{t})e^{\xi^{\pm}\sqrt{1-\nu}} \tag{27a}$$

$$\begin{aligned}\tilde{\psi}_0^{\pm}(\xi^{\pm},\tilde{t}) = {} & \pm A_3(\tilde{t})\frac{1}{1-\nu}e^{-\xi^{\pm}\sqrt{1-\nu}} \\ & \pm A_4(\tilde{t})\frac{1}{1-\nu}e^{\xi^{\pm}\sqrt{1-\nu}} \pm A_5(\tilde{t})\xi^{\pm} \pm A_6(\tilde{t})\end{aligned} \tag{27b}$$

where $A_3(\tilde{t})$, $A_4(\tilde{t})$, $A_5(\tilde{t})$, and $A_6(\tilde{t})$ are unknown functions of time and symmetry is used to obtain a single form for the inner expansions in proximity of the left and right interfaces, similarly to (22b).

D. Outer expansion in the composite layers

In the composite layers, we follow a similar approach to the one presented for the ionomer core. Yet, the asymptotic expansions are modified to account for the difference in the highest power of δ in the modified PNP systems. Specifically, we use the following regular asymptotic expansions for the counterion concentration and electric potential

$$\tilde{c}_{\mathrm{cl}\pm}^{\circ}(r_\pm,\tilde{t}) = \tilde{c}_{\mathrm{cl0}\pm}^{\circ}(r_\pm,\tilde{t}) + \sqrt{\delta}\tilde{c}_{\mathrm{cl1}\pm}^{\circ}(r_\pm,\tilde{t}) + \dots \tag{28a}$$

$$\tilde{\psi}_{\mathrm{cl}\pm}^{\circ}(r_\pm,\tilde{t}) = \tilde{\psi}_{\mathrm{cl0}\pm}^{\circ}(r_\pm,\tilde{t}) + \sqrt{\delta}\tilde{\psi}_{\mathrm{cl1}\pm}^{\circ}(r_\pm,\tilde{t}) + \dots \tag{28b}$$

By replacing (28) into the modified PNP system defined by (18a) and (20b), using the initial conditions (19h), and equating summands with the same power of δ, we find the following general solution for the leading order

$$\tilde{c}^{\circ}_{\mathrm{cl0}\pm}(r_{\pm},\tilde{t}) = 1 \tag{29a}$$

$$\tilde{\psi}^{\circ}_{\mathrm{cl0}\pm}(r_{\pm},\tilde{t}) = \pm B_1(\tilde{t}) r_{\pm} \pm B_2(\tilde{t}) \tag{29b}$$

where $B_1(\tilde{t})$ and $B_2(\tilde{t})$ are unknown functions of time and symmetry is used to obtain a single form for the left and right composite layers.

E. Inner expansions in the composite layers

The inner expansions in the composite layers differ from the expansions in the ionomer core for the following arguments: i) in each composite layer, two boundary layers could develop in the vicinity of the ionomeric membrane and the metal electrode and ii) the largest power of δ in the PNP system for the composite layer is 1.

We start the analysis by studying the ionomer-composite layers interfaces. To this aim, we introduce the local variables

$$\eta^{\pm} = \frac{d^* - r_{\pm}}{\sqrt{\delta}} \tag{30}$$

By substituting the local variables $\eta^{\pm}$ into the modified PNP system defined by (18a) and (20b), we find

$$-\epsilon^* \frac{\partial^2 \tilde{\psi}^{\pm}_{\mathrm{cl}\pm}(\eta^{\pm},\tilde{t})}{\partial(\eta^{\pm})^2} = \delta(\tilde{c}^{\pm}_{\mathrm{cl}\pm}(\eta^{\pm},\tilde{t}) - 1) \tag{31a}$$

$$\frac{\partial \tilde{c}^{\pm}_{\mathrm{cl}\pm}(\eta^{\pm},\tilde{t})}{\partial \tilde{t}} = D^* \left[\frac{1}{1-\nu} \frac{\partial^2 \tilde{c}^{\pm}_{\mathrm{cl}\pm}(\eta^{\pm},\tilde{t})}{\partial(\eta^{\pm})^2} + \frac{\partial^2 \tilde{\psi}^{\pm}_{\mathrm{cl}\pm}(\eta^{\pm},\tilde{t})}{\partial(\eta^{\pm})^2} \right] \tag{31b}$$

where superscripts + and − identify interfaces proximal to $r_+ = d^*$ and $r_- = d^*$, that is, on the right and left of the IPMC, respectively.

We use regular asymptotic expansions for such fields, that is,

$$\tilde{c}^{\pm}_{\mathrm{cl}\pm}(\eta^{\pm},\tilde{t}) = \tilde{c}^{\pm}_{\mathrm{cl0}\pm}(\eta^{\pm},\tilde{t}) + \sqrt{\delta}\tilde{c}^{\pm}_{\mathrm{cl1}\pm}(\eta^{\pm},\tilde{t}) + \dots \tag{32a}$$

$$\tilde{\psi}^{\pm}_{\mathrm{cl}\pm}(\eta^{\pm},\tilde{t}) = \tilde{\psi}^{\pm}_{\mathrm{cl0}\pm}(\eta^{\pm},\tilde{t}) + \sqrt{\delta}\tilde{\psi}^{\pm}_{\mathrm{cl1}\pm}(\eta^{\pm},\tilde{t}) + \dots \tag{32b}$$

By substituting the expansions given by (32) into (31), we find the governing equations for the leading order inner solutions

$$\frac{\partial^2 \tilde{\psi}^{\pm}_{\mathrm{cl0}\pm}(\eta^{\pm},\tilde{t})}{\partial(\eta^{\pm})^2} = 0 \tag{33a}$$

$$\frac{\partial \tilde{c}^{\pm}_{\mathrm{cl0}\pm}(\eta^{\pm},\tilde{t})}{\partial \tilde{t}} = D^* \left[\frac{1}{1-\nu} \frac{\partial^2 \tilde{c}^{\pm}_{\mathrm{cl0}\pm}(\eta^{\pm},\tilde{t})}{\partial(\eta^{\pm})^2} + \frac{\partial^2 \tilde{\psi}^{\pm}_{\mathrm{cl0}\pm}(\eta^{\pm},\tilde{t})}{\partial(\eta^{\pm})^2} \right] \tag{33b}$$

The general solution of (33a) is

$$\tilde{\psi}^{\pm}_{\mathrm{cl0}\pm}(\eta^{\pm},\tilde{t}) = \pm B_3(\tilde{t})\eta^{\pm} \pm B_4(\tilde{t}) \tag{34}$$

where $B_3(\tilde{t})$ and $B_4(\tilde{t})$ are unknown functions of time and symmetry is used to express the solutions in the two composite layers in a compact form. By replacing the Poisson equation (33a) into the linearized modified Nernst-Planck equation (33b), we obtain Fick's second law for the counterion diffusion in the composite layers, see for example [44].

At the interfaces between the composite layers and the electrodes, we use a similar approach by selecting the local variables

$$\zeta^{\pm} = r_{\pm}/\sqrt{\delta} \tag{35}$$

The governing equations are identical to (33) upon replacing $\eta^{\pm}$ with $\zeta^{\pm}$, that is,

$$\frac{\partial^2 \tilde{\psi}^{\mp}_{\mathrm{cl0}\pm}(\zeta^{\pm},\tilde{t})}{\partial(\zeta^{\pm})^2} = 0 \tag{36a}$$

$$\frac{\partial \tilde{c}^{\mp}_{\mathrm{cl0}\pm}(\zeta^{\pm},\tilde{t})}{\partial \tilde{t}} = D^* \left[\frac{1}{1-\nu} \frac{\partial^2 \tilde{c}^{\mp}_{\mathrm{cl0}\pm}(\zeta^{\pm},\tilde{t})}{\partial(\zeta^{\pm})^2} + \frac{\partial^2 \tilde{\psi}^{\mp}_{\mathrm{cl0}\pm}(\zeta^{\pm},\tilde{t})}{\partial(\zeta^{\mp})^2} \right] \tag{36b}$$

In this case, superscripts − and + indicate interfaces proximal to $r_+ = 0$ and $r_- = 0$, that is, on the right and left of the IPMC, respectively. Thus, the electric potential can be analogously written as

$$\tilde{\psi}^{\mp}_{\mathrm{cl0}\pm}(\zeta^{\pm},\tilde{t}) = \pm B_5(\tilde{t})\eta^{\pm} \pm B_6(\tilde{t}) \tag{37}$$

where $B_5(\tilde{t})$ and $B_6(\tilde{t})$ are unknown functions of time. Computing the counterion concentration requires solving a diffusion problem.

F. Matching and boundary conditions

Matching between the leading order outer solutions and the leading order inner solutions within the ionomer core and the two composite layers require satisfying the following conditions

$$\lim_{\xi^{\pm}\to\infty} \tilde{c}^{\pm}_{0}(\xi^{\pm},\tilde{t}) = \lim_{x\to\pm 1} \tilde{c}^{\circ}_{0}(\tilde{x},\tilde{t}) \tag{38a}$$

$$\lim_{\xi^{\pm}\to\infty} \tilde{\psi}^{\pm}_{0}(\xi^{\pm},\tilde{t}) = \lim_{x\to\pm 1} \tilde{\psi}^{\circ}_{0}(\tilde{x},\tilde{t}) \tag{38b}$$

$$\lim_{\eta^{\pm}\to\infty} \tilde{c}^{\pm}_{\mathrm{cl0}\pm}(\eta^{\pm},\tilde{t}) = \lim_{r_{\pm}\to d^*} \tilde{c}^{\circ}_{\mathrm{cl0}\pm}(r_{\pm},\tilde{t}) \tag{38c}$$

$$\lim_{\eta^{\pm}\to\infty}\tilde{\psi}^{\pm}_{\mathrm{cl0}\pm}(\eta^{\pm},\tilde{t})=\lim_{r_{\pm}\to d^{*}}\tilde{\psi}^{\circ}_{\mathrm{cl0}\pm}(r_{\pm},\tilde{t}) \tag{38d}$$

$$\lim_{\zeta^{\pm}\to\infty}\tilde{c}^{\mp}_{\mathrm{cl0}\pm}(\zeta^{\pm},\tilde{t})=\lim_{r_{\pm}\to 0}\tilde{c}^{\circ}_{\mathrm{cl0}\pm}(r_{\pm},\tilde{t}) \tag{38e}$$

$$\lim_{\zeta^{\pm}\to\infty}\tilde{\psi}^{\mp}_{\mathrm{cl0}\pm}(\zeta^{\pm},\tilde{t})=\lim_{r_{\pm}\to 0}\tilde{\psi}^{\circ}_{\mathrm{cl0}\pm}(r_{\pm},\tilde{t}) \tag{38f}$$

By imposing (38a) and (38b) on the concentration and potential profiles given by (22a), (22b), (27a), and (27b), we find the following constraints on the integration constants: $A_4(\tilde{t})=0$, $A_5(\tilde{t})=0$ and $A_6(\tilde{t})=A_1(\tilde{t})$. We note that these conditions imply that the ion flux corresponding to the inner solution of the ionomer is zero at the leading order, see (27). Similarly, by enforcing (38d) and (38f) on the potential profiles in the composite layers in (29b), (34), and (37), we find that $B_3(t)=B_5(t)=0$, $B_4(\tilde{t})=B_1(\tilde{t})d^{*}+B_2(\tilde{t})$, and $B_6(t)=B_2(t)$.

The solution of the diffusion equation for $\tilde{c}^{\mp}_{\mathrm{cl0}\pm}(\zeta^{\pm},\tilde{t})$ in (36) is identically 1 because of the ion blocking condition (19f), the matching condition (38e), the initial condition (19h), and the form of the outer solution in the composite layer in (29a). The solutions for the leading order inner expansions at the electrode-composite layer interfaces are completed by imposing the boundary conditions (19e) to find $B_6(\tilde{t})=\alpha(\tilde{t})/2$.

Differently from the leading order solution in the vicinity of the electrode-composite layer interfaces, the counterion concentration in the proximity of the ionomer-composite layers interface is nontrivial. Specifically, $\tilde{c}^{\pm}_{\mathrm{cl0}\pm}(\eta^{\pm},\tilde{t})$ is computed from the diffusion equation in (36) with boundary condition (19a), matching condition (38c), and initial condition (19h). By substituting the outer solution in the composite layer given by (29a) and the inner solution in the ionomer core in (27a) and by using the general solution given by [65], we obtain

$$\tilde{c}^{\pm}_{\mathrm{cl0}\pm}(\eta^{\pm},\tilde{t})=1\mp\int_{0}^{\tilde{t}}\frac{\mathrm{d}A_3(k)}{\mathrm{d}k}\mathrm{Erfc}\left[\frac{\eta^{\pm}}{\sqrt{4D^{*}\frac{1}{1-\nu}(\tilde{t}-k)}}\right]\mathrm{d}k \tag{39}$$

where $\mathrm{Erfc}(\bullet)$ is the complementary Error function. Beyond the counterion concentration, the electrical potential at the ionomer-composite layers interface should be continuous, that is, (19b) should be satisfied. By using the expression for the inner solutions for the electric potential at such interfaces in (27b) and (34), we obtain $A_1(\tilde{t})+\frac{1}{1-\nu}A_3(\tilde{t})=B_4(\tilde{t})$.

Imposing the boundary conditions (19c) and (19d) requires a different approach due to the variation in the electrical properties at the interface. To this aim, we adapt the procedure presented in [37] for the analysis of ion flux continuity in IPMCs without composite layers. Specifically, we compute the rate of change of the charge stored in the ionomer in the vicinity of composite layers by using (20a), that is,

$$\frac{\partial}{\partial\tilde{t}}\int_{\pm 1}^{\tilde{x}}\tilde{c}(\tilde{x}',\tilde{t})\mathrm{d}\tilde{x}'=\delta\left[\frac{1}{1-\nu}\frac{\partial\tilde{c}(\tilde{x},\tilde{t})}{\partial\tilde{x}}+\frac{\partial\tilde{\psi}(\tilde{x},\tilde{t})}{\partial\tilde{x}}\right]-\delta\left[\frac{1}{1-\nu}\frac{\partial\tilde{c}(\pm 1,\tilde{t})}{\partial\tilde{x}}+\frac{\partial\tilde{\psi}(\pm 1,\tilde{t})}{\partial\tilde{x}}\right] \tag{40}$$

To obtain the sought condition, we move the second term on the right hand side of (40) to the left hand side. Then, we use the inner solution to evaluate the left hand side of the equation and the outer solution for the right hand side. Finally, we take the limit as δ goes to zero while holding $\tilde{x}$ fixed for the inner solutions and $\xi^{\pm}$ fixed for the outer solution. By following this procedure, we obtain the following matching conditions

$$\mp\delta\int_{0}^{\infty}\frac{\partial\tilde{c}^{\pm}(\xi'^{\pm},\tilde{t})}{\partial\tilde{t}}\mathrm{d}\tilde{\xi}'^{\pm}+\left[\frac{1}{1-\nu}\frac{\partial\tilde{c}^{\pm}(0,\tilde{t})}{\partial\xi^{\pm}}+\frac{\partial\tilde{\psi}^{\pm}(0,\tilde{t})}{\partial\xi^{\pm}}\right]=\lim_{\tilde{x}\to\pm 1}\delta\left[\frac{1}{1-\nu}\frac{\partial\tilde{c}^{\circ}(\tilde{x},\tilde{t})}{\partial\tilde{x}}+\frac{\partial\tilde{\psi}^{\circ}(\tilde{x},\tilde{t})}{\partial\tilde{x}}\right] \tag{41}$$

We specialize (41) to the leading order and we simplify each summand as follows. The integral in the left hand side is evaluated by using Poisson's equation (26a) and considering the matching condition for the electric potential (38b) with the outer solution of the electric potential given by (22b). The first summand in the right hand side is written by using the continuity of the ion flux in (19c). The second summand in the right hand side is computed by substituting the expression for the outer solution in (22). Thus, we find the following auxiliary condition

$$\frac{\partial^{2}\tilde{\psi}^{\pm}_{0}(0,\tilde{t})}{\partial\xi^{\pm}\partial\tilde{t}}+D^{*}\phi\left[\frac{1}{1-\nu}\frac{\partial\tilde{c}^{\pm}_{\mathrm{cl0}\pm}(0,\tilde{t})}{\partial\eta^{\pm}}+\frac{\partial\tilde{\psi}^{\pm}_{\mathrm{cl0}\pm}(0,\tilde{t})}{\partial\eta^{\pm}}\right]=\mp A_1(\tilde{t}) \tag{42}$$

Note that the left hand side of (42) corresponds to the current density flowing through to the IPMC defined in (14). A similar result is found in [37], in the absence of composite layers. By replacing (27b), (34), and (39) into (42), we find the following integrodifferential equation for $A_3(\tilde{t})$ and $B_1(\tilde{t})$

$$\frac{\alpha(\tilde{t})}{2}+B_1(\tilde{t})d^{*}-\frac{1}{1-\nu}A_3(\tilde{t})-\theta\frac{1}{\sqrt{1-\nu}}\frac{\mathrm{d}A_3(\tilde{t})}{\mathrm{d}\tilde{t}}=\sqrt{\frac{D^{*}\phi^{2}\frac{1}{1-\nu}}{\pi}}\int_{0}^{\tilde{t}}\frac{1}{\sqrt{\tilde{t}-k}}\frac{\mathrm{d}A_3(k)}{\mathrm{d}k}\mathrm{d}k \tag{43}$$

The initial condition for $A_3(\tilde{t})$ is $A_3(0)=0$ from (19g) and (27a).

To enforce the continuity of the electric displacement at the ionomer-composite layer interfaces, we follow a similar approach. Specifically, we compute the net charge

density in the composite layers in the vicinity of the interfaces by using (18a) to obtain

$$\epsilon^*\left[\frac{\partial\tilde{\psi}_{\mathrm{cl}\pm}(r_\pm,\tilde{t})}{\partial r_\pm}-\frac{\partial\tilde{\psi}_{\mathrm{cl}\pm}(d^*,\tilde{t})}{\partial r_\pm}\right]=\int_{r_\pm}^{d^*}(\tilde{c}_{\mathrm{cl}\pm}(r'_\pm,\tilde{t})-1)\mathrm{d}r'_\pm \quad (44)$$

In order to derive the sought condition, we move the second term on the left hand side of (44) to the right hand side. Then, we use the inner solution to evaluate the right hand side of the equation and the outer solution for the left hand side. We specialize this equation to the leading order and we use (29b) to find

$$-\epsilon^* B_1(\tilde{t})=\sqrt{\delta}\int_0^\infty(\tilde{c}^{\pm}_{\mathrm{cl0}\pm}(\eta^\pm,\tilde{t})-1)\mathrm{d}\eta^\pm+\frac{\epsilon^*}{\sqrt{\delta}}\frac{\partial\tilde{\psi}^{\pm}_{\mathrm{cl0}\pm}(0,\tilde{t})}{\partial\eta^\pm} \quad (45)$$

Now, we utilize (19d) to remove the singularity as δ approaches zero in the last term on the right hand side of (45) so that $\frac{\epsilon^*}{\sqrt{\delta}}\frac{\partial\tilde{\psi}^{\pm}_{\mathrm{cl0}\pm}(0,\tilde{t})}{\partial\eta^\pm}=\frac{\sqrt{\delta}}{\phi}\frac{\partial\tilde{\psi}^{\pm}_{0}(0,\tilde{t})}{\partial\xi^\pm}$. Finally, we substitute (39) and (27b) to obtain the following integral equation

$$-\epsilon^* B_1(\tilde{t})=\sqrt{\delta}\int_0^{\tilde{t}}\frac{\mathrm{d}A_3(k)}{\mathrm{d}k}\frac{\sqrt{4D^*\frac{1}{1-\nu}}}{\sqrt{\pi(\tilde{t}-k)}}\mathrm{d}k+\frac{\sqrt{\delta}}{\phi\sqrt{1-\nu}}A_3(\tilde{t}) \quad (46)$$

By Laplace transforming (43) and (46) and solving for the transformed variables, we finally find

$$\mathcal{L}[A_3](\tilde{s})=\frac{\frac{\mathcal{L}[\alpha](\tilde{s})\sqrt{1-\nu}}{2}}{\frac{1}{\sqrt{1-\nu}}+\sqrt{D^*\phi^2}\sqrt{\tilde{s}}+\tilde{s}+\frac{d^*\sqrt{\delta}}{\epsilon^*}\left(2\sqrt{\frac{D^*}{\tilde{s}}}+\frac{1}{\phi}\right)} \quad (47a)$$

$$\mathcal{L}[B_1](\tilde{s})=\frac{-\frac{\sqrt{\delta}}{\epsilon^*\sqrt{1-\nu}}\left(2\sqrt{\frac{D^*}{\tilde{s}}}+\frac{1}{\phi}\right)\frac{\mathcal{L}[\alpha](\tilde{s})\sqrt{1-\nu}}{2}}{\frac{1}{\sqrt{1-\nu}}+\sqrt{D^*\phi^2}\sqrt{\tilde{s}}+\tilde{s}+\frac{d^*\sqrt{\delta}}{\epsilon^*}\left(2\sqrt{\frac{D^*}{\tilde{s}}}+\frac{1}{\phi}\right)} \quad (47b)$$

where we use $\mathcal{L}[\cdot]$ to identify unilateral Laplace transformation and $\tilde{s}$ as the, dimensionless, Laplace variable. All the other integration constants can be computed from these two quantities based on the relationships presented above, for example,

$$\mathcal{L}[A_1](\tilde{s})=(\sqrt{D^*\phi^2}\sqrt{\tilde{s}}+\tilde{s})\mathcal{L}[A_3](\tilde{s}) \quad (48)$$

G. Composite solution

The composite solutions for the counterion concentration and the electric potential are determined by combining the outer solutions with the inner solutions and by accounting for their common limits, see for example [37]. By following this process, we find

$$\mathcal{L}[\tilde{c}](\tilde{x},\tilde{s})=\frac{1}{\tilde{s}}-\mathcal{L}[A_3](\tilde{s})e^{-\frac{(1-\tilde{x})\sqrt{1-\nu}}{\delta}}+\mathcal{L}[A_3](\tilde{s})e^{-\frac{(1+\tilde{x})\sqrt{1-\nu}}{\delta}} \quad (49a)$$

$$\mathcal{L}[\tilde{\psi}](\tilde{x},\tilde{s})=\mathcal{L}[A_1](\tilde{s})\tilde{x}+\mathcal{L}[A_3](\tilde{s})\frac{1}{1-\nu}e^{-\frac{(1-\tilde{x})\sqrt{1-\nu}}{\delta}}-\mathcal{L}[A_3](\tilde{s})\frac{1}{1-\nu}e^{-\frac{(1+\tilde{x})\sqrt{1-\nu}}{\delta}} \quad (49b)$$

$$\mathcal{L}[\tilde{c}_{\mathrm{cl}\pm}](r_\pm,\tilde{s})=\frac{1}{\tilde{s}}\mp\mathcal{L}[A_3](\tilde{s})e^{-\sqrt{\frac{s(1-\nu)}{D^*}}\frac{d^*\mp r_\pm}{\sqrt{\delta}}} \quad (49c)$$

$$\mathcal{L}[\tilde{\psi}_{\mathrm{cl}\pm}](r_\pm,\tilde{s})=\pm\mathcal{L}[B_1](\tilde{s})r_\pm\pm\frac{\mathcal{L}[\alpha](\tilde{s})}{2} \quad (49d)$$

H. Equivalent circuit model

By using dimensional variables in (42) and assuming that $d\ll h$ for simplicity, we find the following relation between the current through the IPMC and the applied voltage

$$\mathcal{L}[I](s)=\frac{\frac{\epsilon_{\mathrm{i}}\sqrt{1-\nu}}{2\lambda}\left(\frac{\sqrt{D_{\mathrm{d}}}}{\lambda}\sqrt{s}+s\right)}{1+\frac{h\sqrt{D_{\mathrm{d}}(1-\nu)}}{D}\sqrt{s}+\frac{h\lambda\sqrt{1-\nu}}{D}s}\mathcal{L}[V](s) \quad (50)$$

where we introduce the notation $D_{\mathrm{d}}=\phi^2 D_{\mathrm{cl}}$ for the diffusivity in the composite layer scaled by the ionomer volume fraction consistently with [24] and we use s for the dimensional Laplace variable. Therefore, the impedance of the IPMC for small applied voltages $Z(s)$ is written as

$$Z(s)=\frac{\mathcal{L}[V](s)}{\mathcal{L}[I](s)}=\frac{1+(RW)\sqrt{s}+(RC)s}{W\sqrt{s}+Cs} \quad (51)$$

where $C=\frac{\epsilon_{\mathrm{i}}\sqrt{1-\nu}}{2\lambda}$ is the capacitance associated with the double layers in the ionomer, $R=\frac{2h\lambda^2}{\epsilon_{\mathrm{i}}D}$ is the resistance associated with charge transport in the ionomer bulk, and $W=\frac{\epsilon_{\mathrm{i}}\sqrt{D_{\mathrm{d}}(1-\nu)}}{2\lambda^2}$ is the Warburg impedance generated by the charge diffusion in the composite layer. The electric circuit associated with the impedance $Z(s)$ is depicted as Figure 3. Such circuit is a specific instance of the classical Randles circuit in which the resistance associated to the interface is shortcircuited, see for example [44].

We note that the same circuit is derived in [24] without utilizing the method of matched asymptotic expansions. Therein, the exact solution of a linearized PNP system, in which the electron flux in the composite layers is accounted for and steric effects are discarded, is directly approximated. Yet, the numerical values of the capacitance and resistance are different due to steric effects.

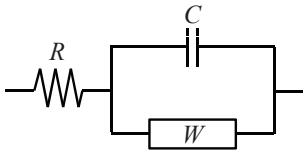

FIG. 3. Equivalent circuit model for small voltage inputs.

IV. ANALYSIS FOR LARGE VOLTAGE INPUTS

The analysis of IPMC charge dynamics in response to a large applied DC voltage with a superimposed small time-varying signal follows the procedure explained in Section III, that is based on the method of matched asymptotic expansions. Differently than the analysis for small input voltages, here we linearize in the neighborhood of a nontrivial chemoeletric solution, which is controlled by the steady state modified PNP system with the DC voltage as the input. Such steady state solution is also determined by using the method of asymptotic expansions. When possible, we thus consolidate the derivation in the following section and we refer to the detailed analysis in Section III.

A. Steady state solution with large DC bias

The modified PNP system for the state state analysis of IPMC response is obtained by setting to zero the ion flux in the ionomer and composite layers given by (16b) and (18b), while retaining the original Poisson's equation where time derivatives are not present. Specifically, in steady state conditions, the modified Nernst-Planck constitutive equations yield

$$\frac{1}{1-\nu\bar{c}(\tilde{x})}\frac{\mathrm{d}\bar{c}(\tilde{x})}{\mathrm{d}\tilde{x}}+\bar{c}(\tilde{x})\frac{\mathrm{d}\bar{\psi}(\tilde{x})}{\mathrm{d}\tilde{x}}=0 \tag{52a}$$

$$\frac{1}{1-\nu\bar{c}_{\mathrm{cl}\pm}(r_\pm)}\frac{\mathrm{d}\bar{c}_{\mathrm{cl}\pm}(r_\pm)}{\mathrm{d}r_\pm}+\bar{c}_{\mathrm{cl}\pm}(r_\pm)\frac{\mathrm{d}\bar{\psi}_{\mathrm{cl}\pm}(r_\pm)}{\mathrm{d}r_\pm}=0 \tag{52b}$$

where we use a superimposed bar to identify steady state variables.

1. Ionomer

By using a regular regular asymptotic expansion for both the counterion concentration and electric potential similarly to (21) in (16a) and (52a) and adapting the initial condition (19g), we obtain the leading order solution

$$\bar{c}_0^{\circ}(\tilde{x})=1 \tag{53a}$$

$$\bar{\psi}_0^{\circ}(\tilde{x})=E_1 \tag{53b}$$

where E_1 is an unknown constant.

Similarly, we modify the local analysis in (23) and (25) to obtain the leading order equations for the inner solutions

$$-\frac{\mathrm{d}^2\bar{\psi}_0^{\pm}(\xi^\pm)}{\mathrm{d}(\xi^\pm)^2}=\bar{c}_0^{\pm}(\xi^\pm)-1 \tag{54a}$$

$$\frac{1}{1-\nu\bar{c}_0^{\pm}(\xi^\pm)}\frac{\mathrm{d}\bar{c}_0^{\pm}(\xi^\pm)}{\mathrm{d}\xi^\pm}+\bar{c}_0^{\pm}(\xi^\pm)\frac{\mathrm{d}\bar{\psi}_0^{\pm}(\xi^\pm)}{\mathrm{d}\xi^\pm}=0 \tag{54b}$$

Following [54], we define the functions $y^\pm(\xi^\pm)$ as

$$\bar{c}_0^{\pm}(\xi^\pm)=\frac{e^{y^\pm(\xi^\pm)}}{1-\nu+\nu e^{y^\pm(\xi^\pm)}} \tag{55}$$

By substituting (55) into the modified Nernst-Planck equation (54b) and integrating, we find

$$\bar{\psi}_0^{\pm}(\xi^\pm)=-y^\pm(\xi^\pm)+E_2^\pm \tag{56}$$

where $E_2^\pm$ are unknown constants. By adapting the matching conditions (38b), we obtain $E_2^\pm=E_1$. Furthermore, by substituting (55) and (56) into (54a), we retrieve a second order nonlinear ordinary differential equation for $y^\pm(\xi^\pm)$, namely, we find

$$\frac{\mathrm{d}^2y^\pm(\xi^\pm)}{\mathrm{d}(\xi^\pm)^2}=\frac{e^{y^\pm(\xi^\pm)}}{1-\nu+\nu e^{y^\pm(\xi^\pm)}}-1 \tag{57}$$

By adapting the matching condition (38a), we have that $y^\pm(\xi^\pm)$ should vanish as $\xi^\pm\to\infty$. Following [54], $y^\pm(\xi^\pm)$ can be univocally computed in terms of $y^\pm(0)$ through the numerical solution of (57). However, $y^\pm(0)$ depends on the steady state chemoelectric behavior in the composite layer as illustrated in what follows.

2. Composite layers

We begin the analysis of the steady state response in each composite layer by studying the inner solutions in the vicinity of both the interfaces using the local variables in (30) and (35). Following the procedure presented in Section III to analyze inner expansions at the ionomer-composite layer and electrode-composite layer interfaces, we find that $\bar{c}_{\mathrm{cl}0\pm}^{\pm}(\eta^\pm)=G_1^\pm$, $\bar{\psi}_{\mathrm{cl}0\pm}^{\pm}(\eta^\pm)=G_2^\pm$, $\bar{c}_{\mathrm{cl}0\pm}^{\mp}(\zeta^\pm)=G_3^\pm$, and $\bar{\psi}_{\mathrm{cl}0\pm}^{\mp}(\zeta^\pm)=G_4^\pm$, where $G_1^\pm$, $G_2^\pm$, $G_3^\pm$, and $G_4^\pm$ are all unknown constants.

By adapting the regular expansion (28) for the steady state outer solution and substituting in the Poisson equation (18a) and the modified Nernst-Planck equation (52b), we find

$$-\epsilon^*\frac{\mathrm{d}^2\bar{\psi}_{\mathrm{cl}0\pm}^{\circ}(r_\pm)}{\mathrm{d}(r_\pm)^2}=\bar{c}_{\mathrm{cl}0\pm}^{\circ}(r_\pm)-1 \tag{58a}$$

$$\frac{1}{1-\nu\bar{c}^{\circ}_{\mathrm{cl}0\pm}(r_\pm)}\frac{\mathrm{d}\bar{c}^{\circ}_{\mathrm{cl}0\pm}(r_\pm)}{\mathrm{d}r_\pm}+\bar{c}^{\circ}_{\mathrm{cl}0\pm}(r_\pm)\frac{\mathrm{d}\bar{\psi}^{\circ}_{\mathrm{cl}0\pm}(r_\pm)}{\mathrm{d}r_\pm}=0 \tag{58b}$$

This problem is similar to the inner solution for the ionomer presented in Section IV A 1. Thus, we introduce the functions $y^{\pm}_{\mathrm{cl}}(r_\pm)$ defined by

$$\bar{c}^{\circ}_{\mathrm{cl}0\pm}(r_\pm)=\frac{e^{y^{\pm}_{\mathrm{cl}}(r_\pm)}}{1-\nu+\nu e^{y^{\pm}_{\mathrm{cl}}(r_\pm)}} \tag{59}$$

Use of these functions yield

$$\bar{\psi}^{\circ}_{\mathrm{cl}0\pm}(r_\pm)=-y^{\pm}_{\mathrm{cl}}(r_\pm)+G^{\pm}_5 \tag{60a}$$

$$\epsilon^*\frac{\mathrm{d}^2y^{\pm}_{\mathrm{cl}}(r_\pm)}{\mathrm{d}(r_\pm)^2}=\frac{e^{y^{\pm}_{\mathrm{cl}}(r_\pm)}}{1-\nu+\nu e^{y^{\pm}_{\mathrm{cl}}(r_\pm)}}-1 \tag{60b}$$

where $G^{\pm}_5$ are unknown constants. Note that in this case, the domain of integration of (60b) is bounded.

By imposing matching conditions (38c), (38d), (38e), and (38f) and the boundary condition (19e), we express all the integration constants $G^{\pm}_1$, $G^{\pm}_2$, $G^{\pm}_3$, and $G^{\pm}_4$ in terms of $G^{\pm}_5$, $y^{\pm}_{\mathrm{cl}}(0)$, and $y^{\pm}_{\mathrm{cl}}(d^*)$. Specifically, we have $G^{\pm}_1=e^{y^{\pm}_{\mathrm{cl}}(d^*)}/(1-\nu+\nu e^{y^{\pm}_{\mathrm{cl}}(d^*)})$, $G^{\pm}_2=-y^{\pm}_{\mathrm{cl}}(d^*)+G^{\pm}_5$, $G^{\pm}_3=e^{y^{\pm}_{\mathrm{cl}}(0)}/(1-\nu+\nu e^{y^{\pm}_{\mathrm{cl}}(0)})$, and $G^{\pm}_4=-y^{\pm}_{\mathrm{cl}}(0)+G^{\pm}_5=\pm\bar{\alpha}/2$, where $\bar{\alpha}$ is the applied large DC voltage $\bar{V}$ nondimensionized with respect to the thermal voltage. Notably, by rearranging these equations, we obtain

$$y^{+}_{\mathrm{cl}}(0)-y^{-}_{\mathrm{cl}}(0)=-\bar{\alpha} \tag{61}$$

3. Boundary conditions

Next, we combine the solutions for the composite layers and the ionomer through the boundary conditions (19a) and (19b) to find $G^{\pm}_5=E_2$ and $y^{\pm}(0)=y^{\pm}_{\mathrm{cl}}(d^*)$. Finally, by imposing the constraint (13) and the boundary condition (19c), we find

$$\frac{\mathrm{d}y^{+}_{\mathrm{cl}}(0)}{\mathrm{d}r_+}=-\frac{\mathrm{d}y^{-}_{\mathrm{cl}}(0)}{\mathrm{d}r_-} \tag{62a}$$

$$\frac{\mathrm{d}y^{\pm}_{\mathrm{cl}}(d^*)}{\mathrm{d}r_\pm}=0 \tag{62b}$$

The functions $y^{\pm}_{\mathrm{cl}}(r^{\pm})$ are obtained by numerically integrating (60b) with boundary conditions (61) and (62). The counterion concentration and electric potential profiles in the ionomer are then computed by solving (57) with $y^{\pm}(0)=y^{\pm}_{\mathrm{cl}}(d^*)$ and $\lim_{\xi^{\pm}\to\infty}y^{\pm}(\xi^{\pm})=0$.

B. Perturbation analysis with DC bias

Here, we investigate IPMC response to a time varying voltage input composed of a large DC bias and a superimposed small time-varying signal by linearizing the modified PNP systems (16) and (18) in the neighborhood of the steady state concentration and electric potential generated by $\bar{\alpha}$. Thus, we write

$$\tilde{c}(\tilde{x},\tilde{t})=\bar{c}(\tilde{x})+\hat{c}(\tilde{x},\tilde{t}) \tag{63a}$$

$$\tilde{\psi}(\tilde{x},\tilde{t})=\bar{\psi}(\tilde{x})+\hat{\psi}(\tilde{x},\tilde{t}) \tag{63b}$$

$$\tilde{c}_{\mathrm{cl}\pm}(r_\pm,\tilde{t})=\bar{c}_{\mathrm{cl}\pm}(r_\pm)+\hat{c}_{\mathrm{cl}\pm}(r_\pm,\tilde{t}) \tag{63c}$$

$$\tilde{\psi}_{\mathrm{cl}\pm}(r_\pm,\tilde{t})=\bar{\psi}_{\mathrm{cl}\pm}(r_\pm)+\hat{\psi}_{\mathrm{cl}\pm}(r_\pm,\tilde{t}) \tag{63d}$$

where a superimposed hat indicates the perturbation with respect to the steady state values. The modified PNP system for the perturbations with respect to steady state is

$$-\delta^2\frac{\partial}{\partial\tilde{x}}\left(\frac{\epsilon(\tilde{x})}{\epsilon_{\mathrm{i}}}\frac{\partial\hat{\psi}(\tilde{x},\tilde{t})}{\partial\tilde{x}}\right)=\hat{c}(\tilde{x},\tilde{t}) \tag{64a}$$

$$\frac{\partial\hat{c}(\tilde{x},\tilde{t})}{\partial\tilde{t}}=\delta\frac{\partial}{\partial\tilde{x}}\left[\frac{1}{1-\nu\bar{c}(\tilde{x})}\frac{\partial\hat{c}(\tilde{x},\tilde{t})}{\partial\tilde{x}}+\frac{\nu\hat{c}(\tilde{x},\tilde{t})}{(1-\nu\bar{c}(\tilde{x}))^2}\frac{\mathrm{d}\bar{c}(\tilde{x})}{\mathrm{d}\tilde{x}}+\hat{c}(\tilde{x},\tilde{t})\frac{\mathrm{d}\bar{\psi}(\tilde{x})}{\mathrm{d}\tilde{x}}+\bar{c}(\tilde{x})\frac{\partial\hat{\psi}(\tilde{x},\tilde{t})}{\partial\tilde{x}}\right] \tag{64b}$$

$$-\epsilon^*\frac{\partial^2\hat{\psi}_{\mathrm{cl}\pm}(r_\pm,\tilde{t})}{\partial(r_\pm)^2}=\hat{c}_{\mathrm{cl}\pm}(r_\pm,\tilde{t}) \tag{64c}$$

$$\frac{\partial\hat{c}_{\mathrm{cl}\pm}(r_\pm,\tilde{t})}{\partial\tilde{t}}=D^*\delta\frac{\partial}{\partial r_\pm}\left[\frac{1}{1-\nu\bar{c}_{\mathrm{cl}\pm}(r_\pm)}\frac{\partial\hat{c}_{\mathrm{cl}\pm}(r_\pm,\tilde{t})}{\partial r_\pm}+\frac{\nu\hat{c}_{\mathrm{cl}\pm}(r_\pm,\tilde{t})}{(1-\nu\bar{c}_{\mathrm{cl}\pm}(r_\pm))^2}\frac{\mathrm{d}\bar{c}_{\mathrm{cl}\pm}(r_\pm)}{\mathrm{d}r_\pm}+\hat{c}_{\mathrm{cl}\pm}(r_\pm,\tilde{t})\frac{\mathrm{d}\bar{\psi}_{\mathrm{cl}\pm}(r_\pm)}{\mathrm{d}r_\pm}+\bar{c}_{\mathrm{cl}\pm}(r_\pm)\frac{\partial\hat{\psi}_{\mathrm{cl}\pm}(r_\pm,\tilde{t})}{\partial r_\pm}\right] \tag{64d}$$

We note that (64) reduces to (16a), (18a), and (20) for null DC voltage.

1. Ionomer

By adapting the regular asymptotic expansion (21) to the perturbations $\hat{c}(\tilde{x},\tilde{t})$ and $\hat{\psi}(\tilde{x},\tilde{t})$ and substituting into (64a) and (64b), we find the leading order outer solutions

$$\hat{c}^{\circ}_0(\tilde{x},\tilde{t})=0 \tag{65a}$$

$$\hat{\psi}^{\circ}_0(\tilde{x},\tilde{t})=H_1(\tilde{t})\tilde{x}+H_2(\tilde{t}) \tag{65b}$$

where $H_1(\tilde{t})$ and $H_2(\tilde{t})$ are unknown functions of time.

The inner solutions are computed by using the local variable (23), adapting the expansion (25), and replacing into (64a) and (64b). To simplify the computation, we make the ansatz that the ion flux in the vicinity of the

polymer-composite layer interface is zero based on the solution for null DC voltage and we later verify that this assumption allows for fulfilling the continuity of the ion flux in (19c) at the leading order. Thus, we have the following leading order equations

$$-\frac{\partial^2\hat{\psi}_0^{\pm}(\xi^{\pm},\tilde{t})}{\partial(\xi^{\pm})^2}=\hat{c}_0^{\pm}(\xi^{\pm},\tilde{t}) \tag{66a}$$

$$\frac{1}{1-\nu\bar{c}_0^{\pm}(\xi^{\pm})}\frac{\partial\hat{c}_0^{\pm}(\xi^{\pm},\tilde{t})}{\partial\xi^{\pm}}+\frac{\nu\hat{c}_0^{\pm}(\xi^{\pm},\tilde{t})}{(1-\nu\bar{c}_0^{\pm}(\xi^{\pm}))^2}\frac{\mathrm{d}\bar{c}_0^{\pm}(\xi^{\pm})}{\mathrm{d}\xi^{\pm}} + \hat{c}_0^{\pm}(\xi^{\pm},\tilde{t})\frac{\mathrm{d}\bar{\psi}_0^{\pm}(\xi^{\pm})}{\mathrm{d}\xi^{\pm}}+\bar{c}_0^{\pm}(\xi^{\pm})\frac{\partial\hat{\psi}_0^{\pm}(\xi^{\pm},\tilde{t})}{\partial\xi^{\pm}}=0 \tag{66b}$$

This system can be conveniently cast in the form of a first order linear system of differential equations for the two dimensional state vector with entries $\beta_1(\xi^{\pm},\tilde{t})=\hat{c}_0^{\pm}(\xi^{\pm},\tilde{t})$ and $\beta_2(\xi^{\pm},\tilde{t})=\frac{\partial\hat{\psi}_0^{\pm}(\xi^{\pm},\tilde{t})}{\partial\xi^{\pm}}$

$$\begin{pmatrix}\frac{\partial\beta_1(\xi^{\pm},\tilde{t})}{\partial\xi^{\pm}}\\ \frac{\partial\beta_2(\xi^{\pm},\tilde{t})}{\partial\xi^{\pm}}\end{pmatrix}=\begin{pmatrix}M_1^{\pm}(\xi^{\pm}) & M_2^{\pm}(\xi^{\pm})\\ -1 & 0\end{pmatrix}\begin{pmatrix}\beta_1(\xi^{\pm},\tilde{t})\\ \beta_2(\xi^{\pm},\tilde{t})\end{pmatrix} \tag{67}$$

where the entries of the state matrix are given by

$$M_1^{\pm}(\xi^{\pm})=-\frac{\nu}{1-\nu\bar{c}_0^{\pm}(\xi^{\pm})}\frac{\mathrm{d}\bar{c}_0^{\pm}(\xi^{\pm})}{\mathrm{d}\xi^{\pm}} - (1-\nu\bar{c}_0^{\pm}(\xi^{\pm}))\frac{\mathrm{d}\bar{\psi}_0^{\pm}(\xi^{\pm})}{\mathrm{d}\xi^{\pm}} \tag{68a}$$

$$M_2^{\pm}(\xi^{\pm})=-(1-\nu\bar{c}_0^{\pm}(\xi^{\pm}))\bar{c}_0^{\pm}(\xi^{\pm}) \tag{68b}$$

The solution of system (67) can be written in the form of a state matrix mapping the value of the state vector at the origin to the values at an arbitrary abscissa. Specifically, we can write

$$\begin{pmatrix}\beta_1(\xi^{\pm},\tilde{t})\\ \beta_2(\xi^{\pm},\tilde{t})\end{pmatrix}=\begin{pmatrix}\Phi_{11}^{\pm}(\xi^{\pm}) & \Phi_{12}^{\pm}(\xi^{\pm})\\ \Phi_{21}^{\pm}(\xi^{\pm}) & \Phi_{22}^{\pm}(\xi^{\pm})\end{pmatrix}\begin{pmatrix}\beta_1(0,\tilde{t})\\ \beta_2(0,\tilde{t})\end{pmatrix} \tag{69}$$

By adapting the matching condition (38a) for the outer solution (65a) and the inner solution given by (69), we obtain

$$\hat{c}_0^{\pm}(0,\tilde{t})=N_1^{\pm}\frac{\partial\hat{\psi}_0^{\pm}(0,\tilde{t})}{\partial\xi^{\pm}} \tag{70}$$

where

$$N_1^{\pm}=\lim_{\xi^{\pm}\to\infty}-\frac{\Phi_{12}^{\pm}(\xi^{\pm})}{\Phi_{11}^{\pm}(\xi^{\pm})} \tag{71}$$

Moreover, by substituting the expression for the counterion concentration at $\xi^{\pm}=0$ given by (70) in (69), integrating as $\xi^{\pm}$ varies from 0 to ∞ and adapting the matching condition (38b) for the outer solution in (65b), we find

$$\hat{\psi}_0^{\pm}(0,\tilde{t})=\pm H_1(\tilde{t})+H_2(\tilde{t})-N_2^{\pm}\frac{\partial\hat{\psi}_0^{\pm}(0,\tilde{t})}{\partial\xi^{\pm}} \tag{72}$$

where

$$N_2^{\pm}=\int_0^{\infty}\Phi_{22}^{\pm}(\gamma)d\gamma+N_1^{\pm}\int_0^{\infty}\Phi_{21}^{\pm}(\gamma)\mathrm{d}\gamma \tag{73}$$

We comment that the functions $N_1^{\pm}$ and $N_2^{\pm}$ are calculated from the state transition matrix in (69), which is, in turn, numerically evaluated from the steady state solution. We also note that if $\bar{\alpha}=0$, that is, the DC bias is null, the state matrix in (67) becomes constant and $N_1^{\pm}=\sqrt{1-\nu}$ and $N_2^{\pm}=1/\sqrt{1-\nu}$.

2. *Composite layers*

The outer solution in the composite layers is obtained by adapting the outer expansion (28) to the analysis of the perturbation of the counterion concentration and electric potential with respect to their steady state values. Specifically, by replacing such regular expansions into the modified PNP system in (64c) and (64d) and following a procedure similar to the one presented in Section III D for null DC voltages, we obtain

$$\hat{c}_{\mathrm{cl0}\pm}^{\circ}(r_{\pm},\tilde{t})=0 \tag{74a}$$

$$\hat{\psi}_{\mathrm{cl}\pm}^{\circ}(r_{\pm},\tilde{t})=K_1^{\pm}(\tilde{t})r_{\pm}+K_2^{\pm}(\tilde{t}) \tag{74b}$$

where $K_1^{\pm}(\tilde{t})$ and $K_2^{\pm}(\tilde{t})$ are unknown functions of time and the initial condition (19h) is taken into consideration.

The analysis of the boundary layers in the vicinity of the two interfaces of each composite layer duplicates the arguments in Section III F. Specifically, we use the local variables (30) and (35) in the modified PNP system (64c) and (64d). By adapting the matching condition (38c) with null outer solution, see (74a) and the initial condition (19h), we obtain

$$\hat{c}_{\mathrm{cl0}\pm}^{\pm}(\eta^{\pm},\tilde{t})=\int_0^{\tilde{t}}\frac{\mathrm{d}K_3^{\pm}(k)}{\mathrm{d}k}\mathrm{Erfc}\left[\frac{\eta^{\pm}}{\sqrt{4D^*(\sigma^{\pm})^2(\tilde{t}-k)}}\right]\mathrm{d}k \tag{75a}$$

$$\hat{\psi}_{\mathrm{cl0}\pm}^{\pm}(\eta^{\pm},\tilde{t})=K_4^{\pm}(\tilde{t})\eta^{\pm}+K_5^{\pm}(\tilde{t}) \tag{75b}$$

$$\hat{c}_{\mathrm{cl0}\pm}^{\mp}(\zeta^{\pm},\tilde{t})=0 \tag{75c}$$

$$\hat{\psi}_{\mathrm{cl0}\pm}^{\mp}(\zeta^{\pm},\tilde{t})=K_6^{\pm}(\tilde{t}) \tag{75d}$$

where $\sigma^{\pm}=\sqrt{1/(1-\nu G_1^{\pm})}$ is computed from the steady state solution analogously to the state transition matrix in (69) and $K_3^{\pm}(\tilde{t})$, $K_4^{\pm}(\tilde{t})$, $K_5^{\pm}(\tilde{t})$, and $K_6^{\pm}(\tilde{t})$ are unknown functions of time. By adapting the matching conditions (38d), (38e), and (38f) with the outer solution given by (74), we find $K_4^{\pm}(\tilde{t})=0$, $K_5^{\pm}(\tilde{t})=K_1^{\pm}(\tilde{t})d^*+K_2^{\pm}(\tilde{t})$, and $K_6^{\pm}(\tilde{t})=K_2^{\pm}(\tilde{t})$.

3. Boundary conditions

By using the boundary conditions (19a), (19b), and (19e) for the fields given by (75) and the values in (70) and (72), we find $K_3^{\pm}(\tilde{t}) = N_1^{\pm}\partial\hat{\psi}_0^{\pm}(0,\tilde{t})/\partial\xi^{\pm}$, $K_5^{\pm}(\tilde{t}) = \pm H_1(\tilde{t}) + H_2(\tilde{t}) - N_2^{\pm}\partial\hat{\psi}_0^{\pm}(0,\tilde{t})/\partial\xi^{\pm}$, and $K_6^{\pm}(\tilde{t}) = \pm\hat{\alpha}(\tilde{t})/2$. Here, $\hat{\alpha}(\tilde{t})$ is the voltage superimposed to the DC value $\tilde{V}(t)$ nondimensionalized with respect to the thermal voltage. We note that the flux continuity in (19c) is automatically satisfied at the leading order through (75a) and (75b) thus verifying the initial ansatz.

Finally, by following the line of arguments in Section III F, we modify the derivations based on (40) and (44) to obtain the following relationships, conveniently written in the Laplace domain,

$$(\tilde{s} + \sqrt{D^*}\phi\sigma^{\pm}N_1^{\pm}\sqrt{\tilde{s}})\frac{\partial\mathcal{L}[\hat{\psi}_0^{\pm}](0,\tilde{s})}{\partial\xi^{\pm}} = \mp\mathcal{L}[H_1](\tilde{s}) \quad (76a)$$

$$-\epsilon^*\mathcal{L}[K_1^{\pm}](\tilde{s}) = \sqrt{\delta}\left(2\sqrt{\frac{D^*}{\tilde{s}}}\sigma^{\pm}N_1^{\pm} + \frac{1}{\phi}\right)\frac{\partial\mathcal{L}[\hat{\psi}_0^{\pm}](0,\tilde{s})}{\partial\xi^{\pm}} \quad (76b)$$

By Laplace transforming (72) and substituting into (76), we find

$$\mathcal{L}[H_1](\tilde{s}) = \frac{\frac{\mathcal{L}[\hat{\alpha}](\tilde{s})}{2}}{1 + U^+(\tilde{s}) + U^-(\tilde{s})} \quad (77a)$$

$$\mathcal{L}[H_2](\tilde{s}) = (U^-(\tilde{s}) - U^+(\tilde{s}))\mathcal{L}[H_1](\tilde{s}) \quad (77b)$$

$$\frac{\partial\mathcal{L}[\hat{\psi}_0^{\pm}](0,\tilde{s})}{\partial\xi^{\pm}} = \mp\frac{\mathcal{L}[H_1](\tilde{s})}{\tilde{s} + \sqrt{D^*}\phi\sigma^{\pm}N_1^{\pm}\sqrt{\tilde{s}}} \quad (77c)$$

where

$$U^{\pm}(\tilde{s}) = \frac{N_2^{\pm} + \frac{d^*\sqrt{\delta}}{\epsilon^*}\left(2\sqrt{\frac{D^*}{\tilde{s}}}\sigma^{\pm}N_1^{\pm} + \frac{1}{\phi}\right)}{2(\tilde{s} + \sqrt{D^*}\phi\sigma^{\pm}N_1^{\pm}\sqrt{\tilde{s}})} \quad (78)$$

In practical terms, once the DC bias is assigned, the steady state solution is computed by following the procedure described in Section IV A and all the parameters $N_1^{\pm}$, $N_2^{\pm}$, and $\sigma^{\pm}$ are consequently calculated. Such parameters ate then used in (77) to compute $H_1(\tilde{t})$ and $H_2(\tilde{t})$ from which all the other pertinent parameters are derived by using the relationships presented above. A composite solution for the counterion concentration and electric potential in the whole IPMC is readily computed by duplicating the arguments in Section III G.

4. Equivalent circuit model

We compute the current flowing through the IPMC in response to the applied voltage $V(t) = \bar{V} + \hat{V}(t)$ by adapting (14). Specifically, we use (72) to calculate the displacement current and we combine (75a), (75b), and (19c) to compute the conduction current. Using dimensional variables and assuming $d \ll h$, the current through the IPMC can be written in the Laplace domain as

$$\mathcal{L}[I](s) = \frac{\frac{\epsilon_{\mathrm{i}}D}{2h\lambda^2}\mathcal{L}[\hat{V}](s)}{1 + \frac{1}{\frac{2h\lambda}{DN_2^+}s + \frac{2h\sqrt{D_{\mathrm{d}}}\sigma^+N_1^+}{DN_2^+}\sqrt{s}} + \frac{1}{\frac{2h\lambda}{DN_2^-}s + \frac{2h\sqrt{D_{\mathrm{d}}}\sigma^-N_1^-}{DN_2^-}\sqrt{s}}} \quad (79)$$

Thus, the IPMC impedance $Z(s) = \mathcal{L}[\hat{V}](s)/\mathcal{L}[I](s)$ corresponds to the lumped circuit model displayed in Figure 4, which consists of a resistor modeling counterion diffusion in the ionomer bulk and two complex impedances quantifying double layer and mass transport phenomena in the vicinity of the anode and the cathode. Namely, we have

$$Z(s) = R + \frac{1}{W^+\sqrt{s} + C^+s} + \frac{1}{W^-\sqrt{s} + C^-s} \quad (80)$$

with

$$R = \frac{2h\lambda^2}{\epsilon_{\mathrm{i}}D} \quad (81a)$$

$$C^{\pm} = \frac{\epsilon_{\mathrm{i}}}{\lambda N_2^{\pm}} \quad (81b)$$

$$W^{\pm} = \frac{\epsilon_{\mathrm{i}}\sqrt{D_{\mathrm{d}}}\sigma^{\pm}N_1^{\pm}}{\lambda^2 N_2^{\pm}} \quad (81c)$$

We note that while the IPMC resistance R is independent of the DC voltage, the capacitances $C^{\pm}$ and Warburg impedances $W^{\pm}$ are all controlled by the DC bias. Specifically, the capacitances and Warburg impedances can be written in terms of the values for null DC offset in Section III H as: $C^{\pm} = \frac{2}{N_2^{\pm}\sqrt{1-\nu}}C$ and $W^{\pm} = \frac{2\sigma^{\pm}N_1^{\pm}}{N_2^{\pm}\sqrt{1-\nu}}W$. Here, the presence of the factor 2 is due to the separation of impedances associated with the cathode and the anode while the presence of the terms $N_1^{\pm}$ and $N_2^{\pm}$ evidences the effect of the DC bias on IPMC impedance. This equivalent model can be assimilated to two Randles circuits with the resistances associated to the interfaces are shortcircuited.

V. RESULTS

A. Verification of the semianalytical solution through finite element results

To offer verification of the proposed semianalytical solution based on matched asymptotic expansions, we compare our predictions on the counterion concentration and

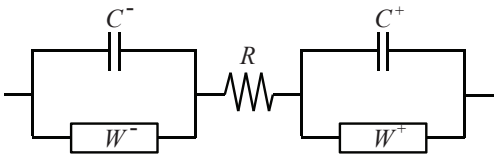

FIG. 4. Equivalent circuit model under large DC bias voltage.

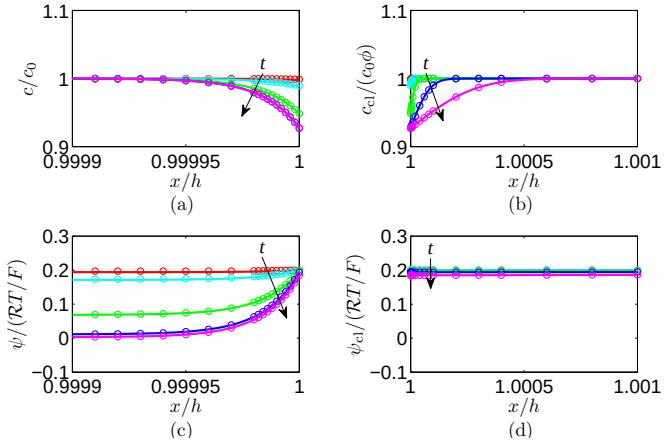

FIG. 5. (Color online) Concentration of counterions and electric potential in the ionomer and the composite layer computed using the proposed semianalytical solution (markers) and the numerical solutions from COMSOL (lines) for $\delta = 10^{-5}$, $\epsilon^* = 1$, $D^* = 1$, $\phi = 0.5$, $d/h = 0.01$, $\nu = 0.6$, and $\alpha = 0.4$. Red (gray), cyan (lightest gray), green (light gray), blue (darkest gray), and purple (dark gray) colors refer to $\tilde{t} = 0.01$, 0.1, 1, 10, and 100, respectively. (a) Counterion concentration in the ionomer; (b) counterion concentration in the composite layer;(c) electric potential in the ionomer; and (d) electric potential in the composite layer.

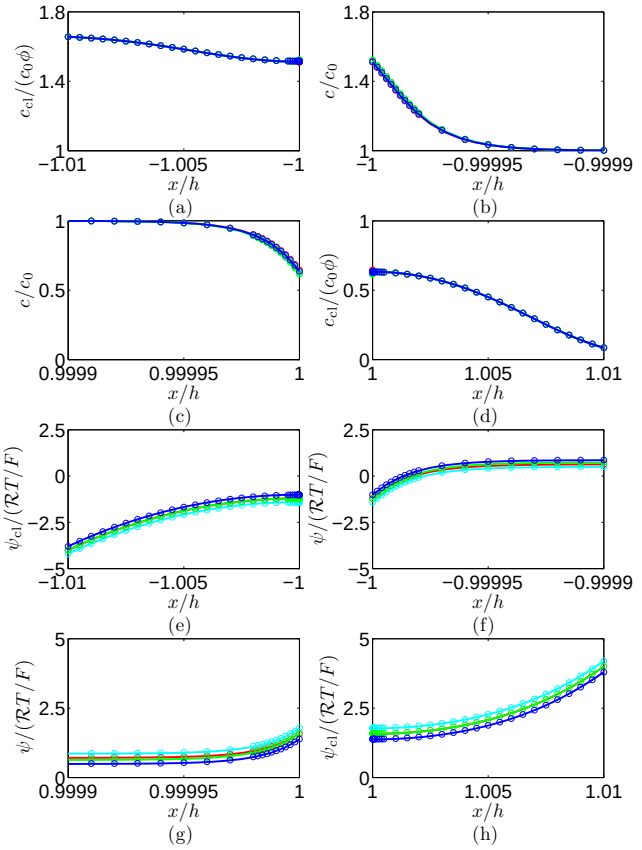

FIG. 6. (Color online) Concentration of counterions and electric potential in the ionomer and the composite layer computed using the proposed semianalytical solution (markers) and the numerical solutions from COMSOL (lines) for $\delta = 10^{-5}$, $\epsilon^* = 1$, $D^* = 1$, $\phi = 0.5$, $d/h = 0.01$, $\nu = 0.6$, and $\alpha(\tilde{t}) = 8 + 0.4\sin(2\pi\tilde{t})$. Red (gray), cyan (lightest gray), green (light gray), and blue (dark gray) colors refer to $\tilde{t} = 1$, 1.25, 1.5, and 1.75, respectively. (a) Concentration of counterions in the composite layer near the cathode; (b) concentration of counterions in the ionomer near the cathode; (c) concentration of counterions in the ionomer near the anode; (d) concentration of counterions in the composite layer near the anode; (e) electric potential in the composite layer near the cathode; (f) electric potential in the ionomer near the cathode; (g) electric potential in the ionomer near the anode; and (h) electric potential in the composite layer near the anode.

the electric potential within the IPMC with finite element results obtained by using the commercial software COMSOL Multiphysics 4.2 [66]. IPMC parameters are selected so that the key dimensionless parameters are $\delta = 10^{-5}$, $\epsilon^* = 1$, $D^* = 1$, $\phi = 0.5$, $d/h = 0.01$, and $\nu = 0.6$. The direct sparse linear system solver MUMPS is used for the finite element implementation and the domain discretization consists of approximately 2000 elements in the ionomer core and 5000 elements in each of the composite layers. Moreover, in the proximity of each interface, meshes are refined to ensure accurate resolution of the boundary layers [67].

As a first benchmark for the semianalytical solution, we compare the predictions obtained in Section III with finite element results computed by implementing the linearized modified PNP system (16a), (18a), and (20). We focus on a step input $\alpha(\tilde{t}) = 0.4$ to elucidate the accuracy of the proposed solution in capturing transient phenomena. Specifically, Figure 5 displays the profiles of the counterion concentration and the electric potential in both the ionomer and the composite layer proximal to the anode. The time snapshots refer to the instants $\tilde{t} = 0.01$, 0.1, 1, 10, and 100. Figure 5 demonstrates the accuracy of the semianalytical solution in predicting the formation of charge boundary layers at the interface between the composite layer and the ionomer, whose thickness is on the order of δ. While the concentration boundary layer in the ionomer has nearly the same length for all instants of time, such length varies in the composite layer due to the counterion diffusion. In the latter, the electric potential is almost constant indicating that capacitive effects in the composite layer are negligible as compared to the double layer capacitance in the ionomer.

Further validation of the proposed approach is pre-

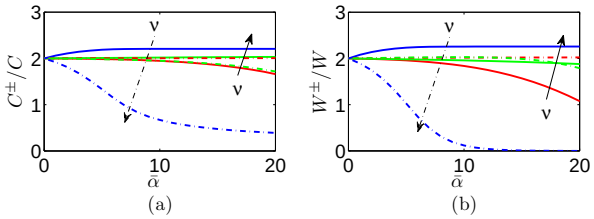

FIG. 7. (Color online) (a) Capacitance at the anode (solid line) and cathode (dash-dotted line) scaled with respect to the value for null DC bias and (b) Warburg impedance at the anode (solid line) and cathode (dash-dotted line) scaled with respect to the value for null DC bias for $\delta = 10^{-5}$, $\epsilon^* = 1$, $D^* = 1$, $\phi = 0.5$, and $d/h = 0.02$. Red (gray), green (light gray), and blue (dark gray) colors refer to $\nu = 0.1$, 0.6 and 0.9, respectively.

sented in Figure 6, where we compare predictions obtained in Section IV with finite element results computed through the analysis of the original nonlinear PNP system in (16) and (18). To differentiate from the step input analysis, we consider a harmonic signal superimposed to a DC bias, namely, we set $\bar{\alpha} = 8$ and $\hat{\alpha}(\tilde{t}) = 0.4\sin(2\pi\tilde{t})$. Beyond illustrating the accuracy of the proposed method, Figure 6 displays a variety of relevant phenomena taking place in IPMC chemoelectrical response. Specifically, Figure 6(a) demonstrates the role played by steric effects in limiting the concentration of the counterions in the vicinity of the electrodes to the relative value of $1/\nu = 1.67$. Comparison of concentration profiles in the vicinity of the anode and the cathode, that is, comparison of Figures 6(a) and 6(b) with Figures 6(c) and 6(d), indicates the presence of a prominent lack of spatial symmetry in the IPMC charge dynamics. This effect is consistent with findings in [28, 36, 37] and is attributed to nonlinear electromigration in the Nernst-Planck equation. In agreement with results for small applied voltage inputs, the electric potential in the composite layers displays a significantly slower variation than the electric potential in the ionomer, indicating that the capacitive behavior is controlled by double layer phenomena developing in the ionomer also at nonzero DC bias.

B. Parametric analysis of the circuit model

Here, we investigate the effect of several key parameters on IPMC chemoelectric behavior. Specifically, we consider the effect of the steric coefficient ν and relative thickness of the composite layer d/h on IPMC impedance as the nondimensional DC voltage $\bar{\alpha}$ is systematically varied. In all the simulations, we select $\delta = 10^{-5}$, $\epsilon^* = 1$, $D^* = 1$, and $\phi = 0.5$. Figure 7 displays both the capacitances and the Warburg impedances for the anode and the cathode with $d/h = 0.02$ as $\bar{\alpha}$ is varied from 0 to 20. Therein, three different values of ν are explored, that is, $\nu = 0.1$, 0.6 and 0.9. For $\nu = 0.1$, the capacitance and Warburg impedance corresponding to the cathode are independent of the DC bias, while increasing the DC bias reduces the capacitance and warburg impedance corresponding to the anode. Overall, this produces a reduction in the IPMC capacitance as predicted by [37, 41, 54] in absence of the composite layers. For $\nu = 0.6$, a similar behavior is observed for the capacitances associated to the anode and the cathode, while the Warburg impedance is largely insensitive to changes in the DC bias. Finally, as ν is increased to $\nu = 0.9$, the overall impedance of the IPMC is controlled by the cathode as the capacitance and Warburg impedance corresponding to the anode are drastically reduced as the DC bias is increased. We comment that if steric effects are marginal, that is, $\nu = 0.1$, the Warburg impedance is bound to decrease in the considered range of DC bias. This behavior can be further elucidated by analyzing the steady state profiles of the counterion concentration and the electric potential for $\bar{\alpha} = 8$ at the three selected values of ν as depicted in Figure 8. Therein, it is demonstrated that the depletion of counterions in the vicinity of the anode and the corresponding counterion enrichment near the cathode are influenced by both the applied DC bias and the steric coefficient ν. Specifically, counterion enrichment in the vicinity of the cathode is drastically limited as ν increases to 0.9 thus reducing IPMC impedance.

Notably, when comparing Figure 6 with Figure 8 we observe that a reduction in the thickness of the composite layer drastically modifies the concentration of counterions and the electric potential profiles in the IPMC. Specifically, as d/h increases charge depletion and enrichment in the ionomer becomes less evident without altering the qualitative behavior of the concentration and electric potential of wider composite layers. The effect of varying d/h is further illustrated in Figure 9 in which we hold $\nu = 0.6$ and we vary d/h to take the values 0.01, 0.02, and 0.04. Therein, it is shown that as d/h and is decreased, both the capacitance and the Warburg impedance associated with the cathode strongly decrease with the DC bias. On the other hand, as the thickness of the composite layer increases the dependence on the DC bias is reduced for both the anode and cathode impedances. For sufficiently thick composite layers, the circuit model in Figure 4 are largely independent of the DC bias.

C. Experiments

To validate the proposed modeling framework based on the modified PNP system and the composite layers' hypothesis, we compare theoretical predictions with experimental results on the impedance of Nafion-based IPMCs neutralized with sodium counterions. We use the same in-house fabricated samples and experimental setup presented in [24]. The explored frequency range is from 0.1 Hz to 10 kHz and the selected DC biases are 0 V,

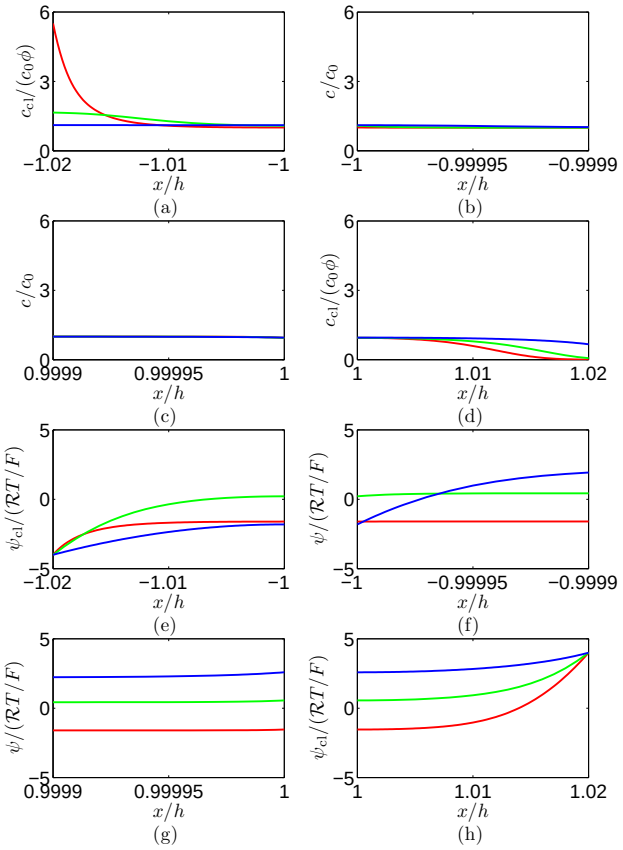

FIG. 8. (Color online) Steady state concentration of counterions and electric potential in the ionomer and the composite layer computed for $\delta = 10^{-5}$, $\epsilon^* = 1$, $D^* = 1$, $\phi = 0.5$, $d/h = 0.02$, and $\bar{\alpha} = 8$. Red (gray), green (light gray), and blue (dark gray) lines refer to $\nu = 0.1$, 0.6 and 0.9, respectively. (a) Concentration of counterions in the composite layer near the cathode; (b) concentration of counterions in the ionomer near the cathode; (c) concentration of counterions in the ionomer near the anode; (d) concentration of counterions in the composite layer near the anode; (e) electric potential in the composite layer near the cathode; (f) electric potential in the ionomer near the cathode; (g) electric potential in the ionomer near the anode; and (h) electric potential in the composite layer near the anode.

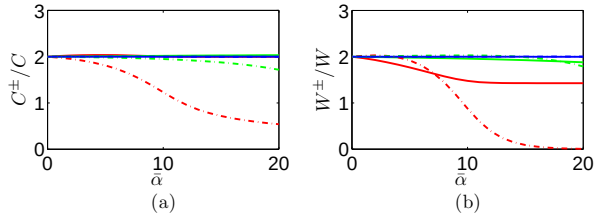

FIG. 9. (Color online) (a) Capacitance at the anode (solid line) and cathode (dash-dotted line) scaled with respect to the value for null DC bias and (b) Warburg impedance at the anode (solid line) and cathode (dash-dotted line) scaled with respect to the value for null DC bias for $\delta = 10^{-5}$, $\epsilon^* = 1$, $D^* = 1$, $\phi = 0.5$, and $\nu = 0.6$. Red (gray), green (light gray), and blue (dark gray) colors refer to $d/h = 0.01$, 0.02, and 0.04, respectively.

0.2 V, and 0.5V so that $\bar{\alpha}$ varies approximately from 0 to 20. Experiments are executed on twelve samples. Each sample is tested at the three different DC biases and tests are 100 s apart. The application of the DC bias is randomized so that each sample is tested in a random order of DC voltages.

Figure 10 displays a representative impedance measurement for a sample from our batch with surface area equal to 1.21 cm^2 and nominal semithickness of the ionomeric membrane $h = 10^{-4}$ m. Visual inspection of the graphs indicates that DC bias is not a determinant of the impedance of the IPMC, which, in turn, suggests that the composite layer has moderate thickness based on Figure 9. Figure 10 also illustrates the predictions of the proposed modeling framework in absence of DC bias, whose equivalent circuit is in Figure 3, with parameters identified through least square error minimization as in [24, 68] from the experimental data for null DC bias. Specifically, we find $R = 3.106\,\Omega$, $C = 0.136$ mF, and $W = 0.0123\,\text{s}^{1/2}\,\Omega^{-1}$. The minimal discrepancy between the experimental data for null DC bias (red solid line) and the model with fitted parameters (black dash-dotted line) is likely due to experimental uncertainties and technical difficulties in measuring IPMC impedance at low frequencies [24].

Salient parameters of the modified PNP model can be extracted from these equivalent circuit properties. Thus, we hypothesize $\nu = 0.25$ (based on a spacing between counterions a equal to 7 Å) and use $F = 96485\,\text{C mol}^{-1}$, $\mathcal{R} = 8.314\,\text{J mol}^{-1}\,\text{K}^{-1}$, $T = 300$ K, $c_0 = 1200\,\text{mol m}^{-3}$, and vacuum permittivity $\epsilon_0 = 8.854 \times 10^{-12}\,\text{F m}^{-1}$ to find $\epsilon_\text{i} = 1.51 \times 10^{-9}$, $D = 1.19 \times 10^{-10}$, and $D_\text{d} = 2.06 \times 10^{-15}$. We comment that the selection of a is informed by the evidence presented in [69] that sodium counterions are surrounded by four water molecules. Notably, these parameter values yield $\delta = 5.8 \times 10^{-6}$ in line with the proposed analysis based on matched asymptotic expansions. Experimental data on DC biases of 0.2 V and 0.5 V can be utilized to bound from below the thickness of the composite layers, see also Figure 9. Specifically, by systematically varying d from 0 to 4.0×10^{-6} m in steps of 0.1×10^{-6} m, we find that the variation of the counterion concentration at both the ionomer-composite layer interfaces as the voltage is changed from 0 to $0.5V$ is less than 1% for $d > 2.3 \times 10^{-6}$ m. Given the secondary effect of the DC bias on the impedance of this IPMC, we expect that composite layers are thicker than 2.3×10^{-6} m. Such prediction is in agreement with scanning electron micrographs reported in [26].

To elucidate on the effect of DC bias on the whole set of 12 IPMCs considered in this work, we perform a statistical analysis of the experimental data by using a one-way analysis of variance (ANOVA) [70]. Specifically, we seek to test the hypothesis of whether the slope of the impedance magnitude in the low frequency limit between 0.1 Hz and 1 Hz varies as the DC bias is changed. The selection of such parameter as compared to the capacitances or Warburg impedances of the equivalent circuit

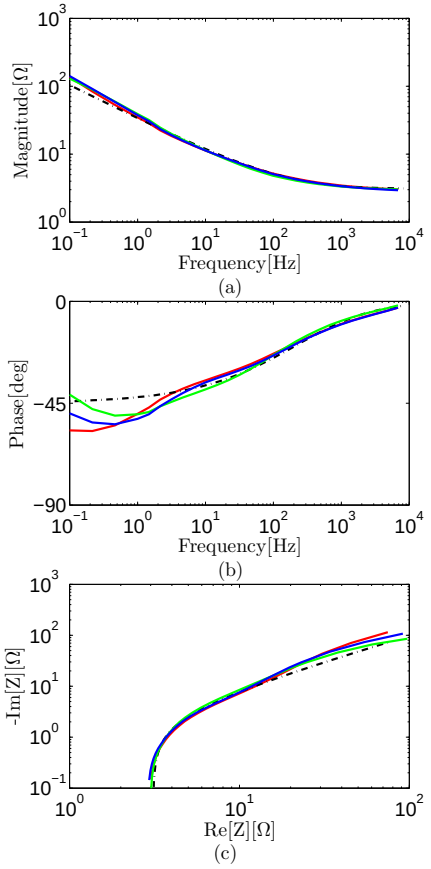

FIG. 10. (Color online) Experimental data on the impedance of a Nafion-based IPMC for DC bias equal to 0 V (red (gray) solid line), 0.2 V (green (light gray) solid line), and 0.5V (blue (dark gray) solid line) and theoretical prediction (black dash-dotted line) of the circuit model in Figure 3 with $R = 3.106\,\Omega$, $C = 0.136\,\text{mF}$, and $W = 0.0123\,\text{s}^{1/2}\,\Omega^{-1}$. Magnitude is in (a), phase in (b), and Nyquist plot in (c).

model in Figure 4 is motivated by the robustness of its identification from the experimental data and its strong dependence on the thickness of the composite layer, as further illustrated in what follows. Table I displays the mean and the standard deviation of such low frequency slope (computed with a population of 12 samples). In the analysis, the DC bias is considered as the independent variable while samples are the dependent variable. Data analysis is carried out using Statview 5.0. The significance level is set at $p \leq 0.05$ for all analyses. Fishers protected least significant difference (PLSD) post-hoc tests are used where a significant main effect of the condition variable is observed. Specifically, DC bias comparisons are found to be similar ($F_{2,33} = 0.52$, $p = 0.5994$), that is, the impedances of the samples for the null DC bias 0 V and the DC biases 0.2 V and 0.5 V do not significantly differ. Post-hoc comparisons reveal that comparing DC bias pairs (0 V vs 0.2 V, 0 V vs 0.5 V, and 0.2 V vs 0.5 V) does not yield significant differences ($p = 0.4359$, 0.347, and 0.8698, respectively). We comment that a similar behavior on Nafion-based IPMCs is also documented in [42] when IPMCs are tested for DC bias not larger than 0.5 V. As the DC voltage is increased to 1 V, noticeable variations in IPMC impedance are therein found, which may possibly be attributed to hydrolysis or chemical reactions at the metal electrodes, see also [41]. Figure 11 displays the experimental data in Table I along with model predictions obtained by using the parameters extracted from the analysis of the sample in Figure 10 (including $\epsilon_\text{i} = 1.51 \times 10^{-9}$, $D = 1.19 \times 10^{-10}$, and $D_\text{d} = 2.06 \times 10^{-15}$) for different values of the thickness of each composite layer. As anticipated earlier, for small values of d the slope of the impedance magnitude changes as the DC voltage is increased towards -20dB/decade, indicating that capacitive effects dominate diffusive phenomena associated with the Warburg impedances. For $d = 2.3 \times 10^{-6}\,\text{m}$, such slope does not vary with the DC voltage and is proximal to -10dB/decade, suggesting that diffusive phenomena are determinants of IPMC charge dynamics.

TABLE I. Experimental data on the low frequency slope of the impedance magnitude of in-house fabricated Nafion-based IPMCs.

DC bias [V]	Mean [-dB/decade]	Std.Dev.
0	10.345	0.920
0.2	10.731	1.326
0.5	10.812	1.308

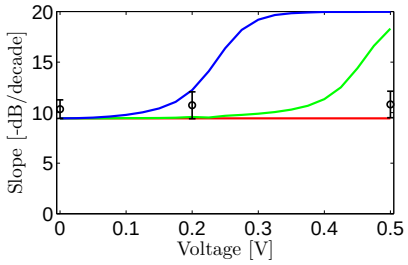

FIG. 11. (Color online) Theoretical predictions of the slope of the impedance magnitude in the low frequency for different values of the DC voltage against experimental results from Table I. Theoretical results are based on parameter values from the sample in Figure 10 and are plotted for $d = 2.3 \times 10^{-6}\,\text{m}$ (red (gray) line), $d = 1.0 \times 10^{-6}\,\text{m}$ (green (light gray) line), and $d = 0.5 \times 10^{-6}\,\text{m}$ (blue (dark gray) line). Open circles are the mean values of the experimental data and error bars refer to standard deviations.

VI. CONCLUSIONS

In this paper, we have analyzed the influence of a DC bias voltage on the chemoelectrical response of IPMCs to a small time-varying voltage input. We have proposed a novel modeling framework based on the modified Poisson-Nernst-Planck system [52–54] and the concept of

composite layers [24]. This approach allows for a comprehensive description of the complex charge dynamics taking place in the vicinity of the IPMC electrodes by accounting for steric effects as well as the presence of dispersed metal particles in the ionomeric membrane.

A semianalytical solution for the counterion concentration and the electric potential in the ionomeric membrane and the composite layers was derived using the method of matched asymptotic expansions. The semianalytical solution allowed for accurately resolving the charge dynamics in the vicinity of the two metal electrodes and establish a tractable equivalent circuit model for the IPMC impedance for a large DC bias. The circuit model comprises the series connection of a resistor, associated to counterion diffusion in the bulk of the IPMC, and two complex elements, related to mass transport and charge accumulation in the vicinity of the electrodes. Each of these two elements consists of the parallel connection of a capacitor and a Warburg impedance. For null DC bias, these two elements are identical and the circuit reduces to the classical Randles model consistently with [24]. On the other hand, for nonzero DC bias, the capacitor and the Warburg impedance corresponding to the anode and the cathode are different and their dependence on the DC bias is controlled by steric effects and counterion diffusion in the composite layer. Notably, we find that such impedances can decrease, increase, or remain nearly constant as the DC bias increase depending on the numerical value of the composite layers' thickness and the steric coefficient.

Implementation of the semianalytical solution to study IPMC chemoelectric behavior requires: i) solving a nonlinear ordinary differential equation for the selected value of DC bias to calculate the counterion concentration and the electric potential at the steady state; ii) calculating pertinent integrals of the counterion concentration to obtain the IPMC impedance and iii) computing an inverse Laplace transform to obtain the the counterion concentration and the electric potential in response to the time-varying superimposed voltage signal. The proposed semianalytical solution was verified using finite element results on the modified Poisson-Nernst-Planck system. Specifically, we compared theoretical predictions on the counterion concentration and electric potential in response to a small step input voltage as well as a small harmonic voltage superimposed to a large DC bias. Further, the proposed modeling framework was validated against experimental results on the impedance of Nafion-based IPMCs.

ACKNOWLEDGEMENTS

This material is based upon work supported by the National Science Foundation under Grant No. CMMI-0926791. The authors thank Mr. Linfeng Shen for his help with IPMC samples fabrication and testing. Also, the authors are grateful to Mr. Giovanni Polverino for his help with the statistic analysis.

[1] E. Biddiss and T. Chau, Medical Engineering and Physics **28**, 568 (2006).
[2] C. Bonomo, L. Fortuna, P. Giannone, S. Graziani, and S. Strazzeri, Smart Materials and Structures **17**, 015014 (2008).
[3] P. Brunetto, L. Fortuna, P. Giannone, S. Graziani, and F. Pagano, IEEE Transactions on Instrumentation and Measurement **59**, 1453 (2010).
[4] Y. Bahramzadeh and M. Shahinpoor, Smart Materials and Structures **20**, 094011 (2011).
[5] K. Park and H.-K. Lee, Journal of the Korean Physical Society **60**, 821 (2012).
[6] T. T. Nguyen, N. S. Goo, V. K. Nguyen, Y. Yoo, and S. Park, Sensors and Actuators A: Physical **141**, 640 (2008).
[7] Z. Chen, S. Shatara, and X. Tan, IEEE/ASME Transactions on Mechatronics **15**, 448 (2010).
[8] M. Aureli, V. Kopman, and M. Porfiri, IEEE/ASME Transactions on Mechatronics **15**, 603 (2010).
[9] S.-W. Yeom and I.-K. Oh, Smart Materials and Structures **18**, 085002 (2009).
[10] Z. Chen, T. I. Um, and H. Bart-Smith, Sensors and Actuators A: Physical **168**, 131 (2011).
[11] K. Abdelnour, A. Stinchcombe, M. Porfiri, J. Zhang, and S. Childress, IEEE/ASME Transactions on Mechatronics **17**, 924 (2012).
[12] J. Brufau-Penella, M. Puig-Vidal, P. Giannone, S. Graziani, and S. Strazzeri, Smart Materials and Structures **17**, 015009 (2008).
[13] R. Tiwari, K. J. Kim, and S. M. Kim, Smart Structures and Systems **4**, 549 (2008).
[14] K. M. Farinholt, N. A. Pedrazas, D. M. Schluneker, D. W. Burt, and C. R. Farrar, Journal of Intelligent Material Systems and Structures **20**, 633 (2009).
[15] M. Aureli, C. Prince, M. Porfiri, and S. D. Peterson, Smart Materials and Structures **19**, 015003 (2010).
[16] A. Giacomello and M. Porfiri, Journal of Applied Physics **109**, 084903 (2011).
[17] S. D. Peterson and M. Porfiri, Applied Physics Letters **100**, 114102 (2012).
[18] Y. Cha, C. N. Phan, and M. Porfiri, Applied Physics Letters **101**, 094103 (2012).
[19] M. Shahinpoor and K. J. Kim, Smart Materials and Structures **10**, 819 (2001).
[20] M. Shahinpoor and M. Mojarrad, *Soft Actuators and Artificial Muscles* (US Patent 6.109.852, issued 29.08.2000.).
[21] K. J. Kim and M. Shahinpoor, Smart Materials and Structures **12**, 65 (2003).
[22] B. J. Akle and D. J. Leo, Smart Materials and Structures **16**, 13481360 (2007).
[23] B. J. Akle and D. J. Leo, Smart Materials and Structures **21**, 105034 (2012).

[24] Y. Cha, M. Aureli, and M. Porfiri, Journal of Applied Physics **111**, 124901 (2012).

[25] S. J. Kim, S.-M. Kim, K. J. Kim, and Y. H. Kim, Smart Materials and Structures **16**, 2286 (2007).

[26] R. Tiwari and K. J. Kim, Applied Physics Letters **97**, 244104 (2010).

[27] P. G. de Gennes, K. Okumura, M. Shahinpoor, and K. J. Kim, Europhysics Letters **50**, 513 (2000).

[28] S. Nemat-Nasser and J. Y. Li, Journal of Applied Physics **87**, 3321 (2000).

[29] G. Del Bufalo, L. Placidi, and M. Porfiri, Smart Materials and Structures **17**, 045010 (2008).

[30] M. Porfiri, Smart Materials and Structures **18**, 015016 (2009).

[31] M. Shahinpoor and K. J. Kim, Smart Materials and Structures **13**, 1362 (2004).

[32] K. Farinholt and D. J. Leo, Mechanics of Materials **36**, 421 (2004).

[33] Z. Chen, X. Tan, A. Will, and C. Ziel, Smart Materials and Structures **16**, 1477 (2007).

[34] U. Zangrilli and L. M. Weiland, Smart Materials and Structures **20**, 094013 (2011).

[35] T. Wallmersperger, D. J. Leo, and C. S. Kothera, Journal of Applied Physics **101**, 024912 (2007).

[36] T. Wallmersperger, B. J. Akle, D. J. Leo, and B. Kröplin, Composites Science and Technology **68**, 1173 (2008).

[37] M. Porfiri, Journal of Applied Physics **104**, 104915 (2008).

[38] M. Aureli, W. Lin, and M. Porfiri, Journal of Applied Physics **105**, 104911 (2009).

[39] J. D. Davidson and N. C. Goulbourne, Journal of Applied Physics **109**, 014909 (2011).

[40] J. D. Davidson and N. C. Goulbourne, Journal of Applied Physics **109**, 084901 (2011).

[41] Z. Chen, D. Hedgepeth, and X. Tan, Smart Materials and Structures **18**, 055008 (2009).

[42] Y. K. Fotsing and X. Tan, Journal of Applied Physics **111**, 124907 (2012).

[43] B. J. Akle, W. Habchi, T. Wallmersperger, E. J. Akle, and D. J. Leo, Journal of Applied Physics **109**, 074509 (2011).

[44] A. J. Bard and L. R. Faulkner, *Electrochemical Methods: Fundamentals and Applications* (John Wiley and Sons, Inc., Hoboken, NJ, 2001).

[45] Y. Liu, R. Zhao, M. Ghaffari, J. Lin, S. Liu, H. Cebeci, R. G. de Villoria, R. Montazami, D. Wang, B. L. Wardle, J. R. Heflin, and Q. Zhang, Sensors and Actuators A: Physical **181**, 70 (2012).

[46] S. Leary and Y. Bar-Cohen, in *Proceedings of SPIE's Annual International Symposium on Smart Structures and Materials* (1999) pp. 81–86.

[47] K. Newbury and D. J. Leo, Journal of Intelligent Material Systems and Structures **14**, 343 (2003).

[48] K. Farinholt and D. J. Leo, Journal of Applied Physics **104**, 014512 (2008).

[49] X. Bao, Y. Bar-Cohen, and S. Li, in *Proceedings of the SPIE Smart Structures and Materials Symposium, EAPAD Conference* (2002) pp. 220–227.

[50] J. W. Paquette, K. J. Kim, J.-D. Nam, and Y. S. Tak, Journal of Intelligent Material Systems and Structures **14**, 633 (2003).

[51] C. Bonomo, L. Fortuna, P. Giannone, and S. Graziani, IEEE Transactions on Circuits and Systems I **53**, 338 (2006).

[52] M. S. Kilic, M. Z. Bazant, and A. Ajdari, Physical Review E **75**, 021502 (2007).

[53] M. S. Kilic, M. Z. Bazant, and A. Ajdari, Physical Review E **75**, 021503 (2007).

[54] M. Porfiri, Physical Review E **79**, 041503 (2009).

[55] M. Z. Bazant, M. S. Kilic, B. D. Storey, and A. Ajdari, Advances in Colloid and Interface Science **152**, 48 (2009).

[56] N. Abaid, R. S. Eisenberg, and W. Liu, SIAM Journal of Applied Dynamical Systems **7**, 1507 (2008).

[57] M. Z. Bazant, K. T. Chu, and B. J. Bayly, SIAM Journal of Applied Mathematics **65**, 1463 (2005).

[58] K. T. Chu and M. Z. Bazant, SIAM Journal of Applied Mathematics **65**, 1485 (2005).

[59] V. Barcilon, D.-P. Chen, R. Eisenberg, and J. Jerome, SIAM Journal on Applied Mathematics **57**, 631 (1997), http://epubs.siam.org/doi/pdf/10.1137/S0036139995312149.

[60] B. Eisenberg and W. Liu, SIAM Journal of Mathematical Analysis **38**, 1932 (2007).

[61] A. H. Nayfeh, *Perturbation Methods* (Wiley-VCH, Germany, 2004).

[62] T. R. Ferguson and M. Z. Bazant, Journal of the Electrochemical Society **159**, A1967 (2012).

[63] J. Park and J. Jerome, SIAM Journal on Applied Mathematics **57**, 609 (1997).

[64] D. K. Cheng, *Field and Wave Electromagnetics* (Addison Wesley, Boston, 1989).

[65] W. A. Strauss, *Partial differential equations* (John Wiley & Sons, Inc., New Jersey, 1992).

[66] *http://www.comsol.com/*.

[67] M. Aureli and M. Porfiri, Smart Materials and Structures **21**, 105030 (2012).

[68] A.-K. Hjelm and G. Lindbergh, Electrochimica Acta **47**, 1747 (2002).

[69] W. J. Yoon, P. G. Reinhall, and E. J. Seibel, Sensors and Actuators A: Physical **133**, 506 (2007).

[70] C. M. Judd, G. H. McClelland, and C. S. Ryan, *Data analysis: A model comparison approach* (Routledge/Taylor & Francis Group, New York, 2009).